5-2017

Discrete Element Analysis of SCB Variability: Asphalt Mixtures

David Saul Renteria
The University of Texas Rio Grande Valley

DISCRETE ELEMENT ANALYSIS OF SCB VARIABILITY – ASPHALT MIXTURES

A Thesis

by

DAVID SAUL RENTERIA

Submitted to the Graduate College of
The University of Texas Rio Grande Valley
In partial fulfillment of the requirements for the degree of

MASTER OF SCIENCE ENGINEERING

May 2017

Major Subject: Mechanical Engineering

DISCRETE ELEMENT ANALYSIS OF SCB VARIABILITY – ASPHALT MIXTURES

A Thesis
by
DAVID SAUL RENTERIA

COMMITTEE MEMBERS

Dr. Constantine Tarawneh
Chair of Committee

Dr. Robert Jones
Committee Member

Dr. Aaron Greenwood
Committee Member

May 2017

ABSTRACT

Renteria, David Saul, Discrete Element Analysis of SCB Variability – Asphalt Mixtures. Master of Science Engineering (MSE), May, 2017, 71 pp., 8 tables, 41 figures, references, 45 titles.

The Semi-Circular Bending (SCB) test was modeled using the Discrete Element Method (DEM) implemented in numerical software Particle Flow Code (PFC). The fracture analysis of the SCB was studied using two mixtures gradation, Superpave, and Coarse Matrix High Binder. The aggregate phase in the model was achieved by using two-dimensional aggregate images with different angularity indexes. The study of the variability of the SCB extends to the random generation of aggregate particles and air voids in the model, in addition to changing the properties at the interface between the aggregate and mastic phases. Results indicate the strong influence of the location of aggregates and air voids in the crack initiation and propagation. Moreover, the interface properties have a significant effect on the performance of asphalt mixtures. The SCB implemented in DEM can be considered as a repeatable cracking test based on the coefficient variation.

DEDICATION

I would like to dedicate this thesis to the savior of my soul. Your grace and unlimited mercy gave me the strength and patience that I needed throughout these past years to complete this work. Thank you, God. To my family, your sacrifices and support have motivated me to accomplish this master's degree. Thank you for believing in me.

ACKNOWLEDGEMENTS

There are no words that can be put in a sentence to describe how deeply grateful I feel to Dr. Enad Mahmoud. Since day one you have always shown patience, attention, and willingness to help me to succeed in my professional career. Your constant support and guidance were essential in continuing my graduate studies. I will always be in debt with you for everything you did for me as an undergraduate and graduate student; thank you very much for your time. This gratitude is also shared to Dr. Constantine Tarawneh who was the person who put me in contact with Dr. Enad Mahmoud. Moreover, I would like to express my acknowledgement to Dr. Constantine Tarawneh for his assistance and interest in supervising my thesis work in spite of his very tight schedule and numerous commitments to fifteen other students in his research team.

Finally, I would like to thank Dr. Aaron Greenwood for always being a person who cares and shows enthusiasm over other's people work. You clearly made a positive impact in my life; thank you for your cooperation and time spent on editing and revising my thesis.

TABLE OF CONTENTS

Page

ABSTRACT iii

DEDICATION iv

ACKNOWLEDGMENTS v

TABLE OF CONTENTS vi

LIST OF TABLES vii

LIST OF FIGURES viii

CHAPTER I. INTRODUCTION 1

CHAPTER II. LITERATURE REVIEW 3

CHAPTER III. METHODOLOGY 13

Classification of Low and High Angular Aggregates 16

Generation of Aggregate Clumps 20

Representation of Aggregate, Mastic, and Air Void Phases 26

Contact Properties 30

Boundary Conditions 35

Loading 35

CHAPTER IV. RESULTS AND DISCUSSION 37

Simulation Results with Interface Properties Mastic-Mastic 42

Simulation Results with Interface Properties Twice Mastic 50

CHAPTER V. CONCLUSIONS AND FUTURE WORK 64

REFERENCES 67

BIBLIOGRAPHY 71

LIST OF TABLES

Page

Table 1: Angularity Classification for BMD, AMD, and Combined 17

Table 2: Percentage of Asphalt Mixtures Components 22

Table 3: Gradation Test for CMHB and Superpave Mixtures 23

Table 4: New Gradation Test for CMHB and Superpave Mixtures 23

Table 5: Comparison of Experimental and Modeling Results of Asphalt Mixtures 34

Table 6: Asphalt Mixtures Generated to Study the Variability of the SCB 34

Table 7: Coefficient of Variation for CMHB Mixtures 59

Table 8: Coefficient of Variation for Superpave Mixtures 60

LIST OF FIGURES

Page

Figure 1: Particle Flow Code Software Model Components 14
Figure 2: Rheological Components of the Linear Contact Bond Model 15
Figure 3: Rheological Components of the Burger's Model 15
Figure 4: Angularity Index of Low-Angularity Aggregates 17
Figure 5: Low-Angularity Aggregates 18
Figure 6: Angularity Index of High-Angularity Aggregates 19
Figure 7: High-Angularity Aggregates 20
Figure 8: Volumetric Relationship of the Asphalt Mixtures 21
Figure 9: Aggregate Generation 24
Figure 10: CMHB Aggregate Generation 25
Figure 11: Superpave Aggregate Generation 26
Figure 12: Generation of the SCB Model 28
Figure 13: SCB Model 29
Figure 14: Heterogeneous SCB Model 30
Figure 15: Aggregate Calibration Tests 32
Figure 16: Internal Structure of Asphalt Mixtures 33
Figure 17: SCB Model with Supports 35
Figure 18: Wall Speed Study 36
Figure 19: CMHB Mixture Simulations 38
Figure 20: Variability of Aggregate Angularity in CMHB Mixtures 39

Figure 21: Superpave Mixture Simulations 40
Figure 22: Variability of Aggregate Angularity in Superpave Mixtures 41
Figure 23: Superpave and CMHB Simulations 42
Figure 24: CMHB and Superpave Simulations – High Aggregate Angularity 43
Figure 25: CMHB Samples – Aggregate Property 45
Figure 26: Cracking in CMHB – Granite Sample 45
Figure 27: Force – Displacement Graph for CMHB Granite Sample 46
Figure 28: CMHB and Superpave Simulations – Low Aggregate Angularity 47
Figure 29: Superpave Samples - Aggregate Property 48
Figure 30: Cracking in Superpave – Granite Sample.....49
Figure 31: Cracking in CMHB – Granite Sample.....50
Figure 32: Superpave and CMHB Simulations – Modified Interface.....51
Figure 33: CMHB and Superpave Simulations – High Aggregate Angularity.....52
Figure 34: CMHB Samples - Aggregate Property 53
Figure 35: Cracking in Superpave – Granite Sample – Modified Interface.....54
Figure 36: Force – Displacement Graph for CMHB – Granite Sample – Modified Interface.....54
Figure 37: Cracking in CMHB – Granite Sample – Modified Interface.....55
Figure 38: CMHB and Superpave Simulations – Low Aggregate Angularity 56
Figure 39: Cracking in Superpave – Granite Sample – Modified Interface.....56
Figure 40: Superpave – Granite Properties – Low Angularity Index – Modified Properties 57
Figure 41: Plot Showing the 95% Confidence Interval.....61

CHAPTER I

INTRODUCTION

Asphalt concrete pavements are placed on a granular base layer, which at the same time is supported by compacted soil or also known as the subgrade. This type of pavement comprises a large part of both rural and urban pavements in the United States. Due to this, the performance of asphalt pavements under different conditions is of special interest among highways agencies since millions of dollars are being spent on maintenance and rehabilitation every year.

The asphalt concrete mixture is mainly composed of coarse aggregate, asphalt binder, and air voids. Aggregates come from natural rocks in which the primary interest when selecting them for asphalt pavement is based on their texture, shape, and angularity. Moreover, the resistance of asphalt mixtures to fracture depends primarily on good aggregate-to-aggregate contact, aggregate properties, and the type of gradation size used. Asphalt binder is obtained from crude petroleum by the distillation process. It is a highly viscous material, thus, their mechanical performance is a function of time and temperature. Mastic is referred to asphalt binder mixed with fine aggregates passing No. 16 sieve. Air voids in the mixture are controlled according to the method of compaction and gradation used, and their main function is to provide a good drainage system. All these components are crucial in the design of asphalt pavements, not to mention other additives which might increase the performance of asphalt mixtures and reduce the problems related to fracture. However, the individual performance of mastic and aggregates is not the same when

these components are mixed together. Since pavement deterioration is attributed from traffic loads and environmental conditions, there are different asphalt pavement mixtures designs available to use that provide an adequate performance depending on the project needs. Therefore, the properties of aggregate, asphalt binder and their relationship is of primary interest in the pavement design process. Furthermore, many researchers have been focused on developing laboratory tests that could provide insights into the performance of asphalt pavements.

Rutting and reflective cracking are the major distress occurring in Hot Mix Asphalt (HMA) pavements due to heavy truck loads inducing high tensile strains. Researchers and practitioners have been employed different crack test methods to characterize the fracture resistance of HMA such as Indirect tensile test (IDT), Overlay tester (OT), Semi-circular bending test (SCB) and disk-shaped compaction test (DSCTT). This study adopts the numerical modeling of the SCB to analyze and understand the fracture behavior of different asphalt mixtures considering the random generation of aggregates and air voids in the mixture. These factors affect the variability of the SCB test, in addition to the contact properties at the interface. The capability of the numerically SCB test to assist in the investigation of the fracture analysis of asphalt mixtures is demonstrated in this work.

CHAPTER II

LITERATURE REVIEW

There is extensive literature on the Semi-Circular Bending (SCB) test for fracture characterization of asphalt mixtures. An overall review of the utilization of the SCB test was given by Saha and Biligir (2015). This article encompasses the analytical procedures as well as the fundamental assessment of fracture performance of asphalt mixtures using the SCB test. It was concluded that the SCB test was found to be a potential cracking test to assist in the fracture analysis of asphalt mixtures.

Based on the current literature, the modeling methods for the SCB test have been concentrated in two main approaches, the Discrete Element Method (DEM) and the Finite Element Method (FEM). Different contact models simulating the behavior of brittle and viscoelastic materials have been proposed for DEM and FEM. Additionally, several techniques for representing the aggregate, air void, and mastic phases within the mixture have been developed in the past decade.

The contact force chains developed in asphalt mixtures during loading provide insight into the interactions of the asphalt concrete constituents. Proper selection of contact models available in the numerical software is critical for representing actual material behavior. Pei et al. (2013) generated a two-dimensional (2D) DEM of asphalt specimens from image processing techniques to analyze the force chain network in the mixture. Some of the findings state that

when the maximum load was applied to the specimens, the maximum contact force was observed in the aggregate material, followed by the interface (between aggregate and sand mastic) and sand mastic. Dondi et al. (2014) also studied the internal contacts in asphalt mixtures using a three-dimensional (3D) discrete element model (DEM). The study focuses on capturing the bitumen behavior at different temperatures and frequencies. Results of the numerical simulation agreed with laboratory tests. Cai et al. (2014) applied the Burger's model to recreate the uniaxial compression test. The 3D model was capable of simulating the compression test for asphalt mixtures using the Discrete Element Method. Ren and Sun (2015) utilized the DEM elastic contact model and Maxwell viscoelastic contact models for bonding aggregates and asphalt mastic, respectively. Feng et al. (2015) studied the viscoelastic behavior of asphalt mixtures using a 3D discrete element simulation. The project was divided into two phases. The first phase consisted of obtaining the complex modulus of asphalt mixtures by performing some laboratory tests. The Burger's contact model input parameters implemented in the simulation were calibrated based on the laboratory results. The second phase consisted of validating the 3D numerical model results with those measured in the laboratory. Authors concluded that the computer simulations predicted the results from the laboratory tests.

In DEM, X-ray computed tomography (CT) imaging technique has been used to capture the aggregate material from asphalt samples into the numerical model. The fracture behavior of homogeneous and heterogeneous 2D Discrete Element Model (DEM) simulating the disk – shaped compact tension (DC (T)) test was done by Kim et al. (2008). The generation of the aggregate material in the heterogeneous model was done using high – resolution image technique. Cohesive zone models were implemented in both tests to analyze the crack propagation. Material properties were given for aggregate, mastic and the interface between

aggregate and mastic. Overall, both tests showed good correlation regarding the peak load and initial stiffness from laboratory tests.

You et al. (2009) used the X-Ray computed tomography (CT) imaging technique to develop a heterogeneous 3D and 2D distinct element models. Aggregate, mastic, and air voids were included in both models. The mastic phase was a combination of asphalt binder and aggregate material passing sieve size 2.36 mm. It was concluded that the mixture modulus of the 3D DEM model matched the laboratory results for different temperatures and loading frequencies. Furthermore, Kim et al. (2009) monitored the fracture behavior of asphalt concrete using a 2D clustered DEM single – edge notched beam (SENB) test. The generation of the aggregate phase in the heterogeneous model was done using imaging techniques. Homogeneous and heterogeneous models were analyzed under mode I and mode II fracture behavior, respectively. A cohesive zone model (CZM) was used to simulate the fracture process. Cracking in the heterogeneous model was predicted well, while for the homogeneous model, the energy decomposition results showed that the friction, strain, and fracture energies were dominant in the fracture test.

Years later, Zelelew and Papagiannakis (2011) developed an automated digital image processing (DIP) technique to successfully characterize the asphalt mixture phases from X-ray CT images. The proportions of the aggregate, mastic, and air voids from the X-ray images were similar with respect to the asphalt concrete cores; therefore, they can be directly entered in computer simulations for further study. Deyu et al. (2011) developed a 2D virtual rutting test using the Discrete Element Method (DEM). Coarse aggregate phase was also generated within the model using a digital image processing technique to account for aggregate angularity. In addition, the air void phase was also part of this study. The deformation law results were similar

with the experimental tests. Additionally, the model was able to predict the behavior of asphalt mixtures under high temperature. More recently, Khattak et al. (2014) developed a 2D model of hot mix asphalt (HMA) and asphalt matrix (AM). The capture of the aggregate and mastic phases was done using imaging techniques. The dynamic modulus and strength of neat asphalt mixtures and carbon nanofibers (CNF) modified HMA mixtures from the numerical simulations were compared with laboratory results. The authors observed that the mechanical performance of virtual asphalt mixtures modified with CNF exhibited similar behavior to that observed in the laboratory data.

Another approach for generating aggregate particles different from the digital image-based method has been proposed by Hou and Zhang (2015). This new method consists of a series of algorithms based on the probability analysis. In addition to the generation of aggregates, the suggested method calculates the number of 2D aggregates in the 2D mixture. A powerful digital three-dimensional algorithm was also developed by Liu et al. (2015) to generate aggregate particles with a different shape, fracture surface, and angularity. This algorithm is also capable of producing air voids and asphalt mastic for asphalt mixtures.

The strain energy release rate of nine different asphalt mixtures across the state of Louisiana were analyzed by Mohammad et al. (2012). These asphalt mixtures contained four types of asphalt binders and two nominal maximum aggregate sizes. The SCB test was used to obtain the field cracking rate and compare it with the strain energy release rate for each mixture. Based on the results, it was concluded that the SCB test could be used to evaluate the fracture resistance of asphalt pavements. Biligiri et al. (2012) investigated the crack propagation in the SCB test for two laboratory asphalt mixtures to get an insight on the fracture crack propagation. Also, field core samples were studied based on the laboratory test methodology. For both

approaches, important conclusions were drawn regarding the increase of asphalt content in the mixture.

Numerical and experimental asphalt pavement tests at low temperatures have been studied by several researchers. Li and Marasteanu (2010) conducted the SCB test at three different low temperatures to evaluate the fracture resistance of six different asphalt mixtures. The following parameters were studied: binder type, aggregate type, binder modifier, and air voids. Additionally, two loading conditions and initial notch lengths were also part of this study. Results showed that the aggregate type and air void content significantly affects the fracture response of asphalt mixtures. Furthermore, it was seen that the modified asphalt binder increases the fracture energy of asphalt mixtures for the two lowest temperature values. For the effect of the test temperature, the highest fracture energy occurred at -30°C, which is the lowest temperature tested for the SCB. Also, low coefficient of variation was collected from three replicates. Perez et al. (2013) evaluated the SCB test by changing the load application time and temperature for asphalt mixtures. The research team concluded that as the temperature decreases, the properties of bituminous mixtures decreases. Furthermore, the coefficient of variation was below 15% for the laboratory asphalt results. The determination of creep compliance at low temperatures for asphalt mixtures was proposed by Teshale et al. (2013). Numerical and experimental simulations were conducted for this study. The research findings demonstrate that the SCB test was capable of determining the characterization of asphalt mixtures at low temperatures.

The major challenge in aggregate modeling is to include certain aggregate characteristics such as texture, angularity, and form. Yu and Shen (2011) conducted a study to determine the effect of aggregate packing on the dynamic modulus of HMA mixtures. The aggregate shape and angularity were represented by using clumps. A 3D discrete element method (DEM) model was

used to randomly generate aggregate material larger than No. 16 sieve. It was found that as the particle angularity increases, the stiffness of the asphalt mixture increases as well due to the particle interlock within the mixture. Dondi et al. (2012) also studied the effect of the aggregate angularity by recreating a triaxial test in numerical software. The 3D model results showed a correlation between the aggregate angularity and the performance of the test. The increase in the aggregate angularity yields more interlocking of aggregates, more aggregate contacts, and a uniform distribution of internal forces.

It has been found that the air void content also affects the performance of asphalt mixtures. Chen et al. (2013) examined the air void distribution in compaction processes such as Superpave gyratory compactor (SGC) and vibratory compactor by using the DEM. The compaction method, gradation size, and mold height were some of the factors in consideration for this study. Results indicated that the SGC specimens resulted with more homogeneous air voids than vibratory compactor specimen. Moreover, the aggregate gradation plays a significant role in the vertical air void distribution. More recently, Ma et al. (2016) studied the impact of air void phase in asphalt mixtures by conducting a uniaxial static creep 3D model test. The effects of the air void content, size, and orientation on the asphalt mixtures behavior were analyzed. After evaluating the computer simulation results, it was concluded that as the air void content increases, the asphalt mixtures experienced greater creep strain. Additionally, a nonuniform distribution of air voids within the mixture causes negative effects on the creep behavior of asphalt mixtures.

It is notable that the aggregate characteristics and properties play an important role in response to the induced loading in asphalt mixtures. Nanoindentation has been proven to be a useful technique to characterize the material properties for aggregate and asphalt phases.

Khorasani et al. (2013) used this technique to analyze the elastic modulus and hardness values for aggregate, mastic, and interface zone (between mastic and aggregate). Results showed that the elastic modulus and hardness values for the interface zone were in between the mastic and aggregate phases. Authors concluded that the results for the interface can be used in micromechanical numerical models as input for interface properties.

The semi-circular bending test has been applicable in determining the loading mode I, mode II, and mixed mode I/II for brittle materials. Ayatollahi and Aliha (2006) determined the values for mode II fracture toughness using a modified criterion for rock material and a brittle polymer. Pirmohammad and Ayatollahi (2013) also studied the effect of loading modes (mode I, mode II, and mixed mode I/II) and test temperature (0°C, -10°C, -20°C and -35°C) in the SCB test for modified and normal asphalt mixtures. The crack paths for mode I and mode II were straight and curvilinear, respectively. In addition, the test temperature significantly affects the fracture resistance of both normal and modified asphalt mixtures. However, the modified asphalt mixtures showed better fracture resistance at temperatures below -20°C. Also, Kuruppu and Chong (2013) utilized the SCB test method to determine the fracture toughness of brittle materials. Their work presented formulations for calculating mode I and mixed mode fracture. The SCB test was considered to be a suitable test for obtaining the fracture toughness of rock at high strain rates.

Aliha et al. (2014) studied the fracture behavior for different asphalt mixtures using the SBC test in mode II. The effect of aggregate type, air void content, aggregate size, and binder type on the critical stress intensity factor was the main objective of this study. Some of the most relevant findings were that having a greater nominal maximum aggregate size (NMAS) increases the fracture resistance of the mixture, and having higher air void content in the mixture reduces

the fracture toughness of the asphalt mixtures. In a different project, four different loading modes were performed using the SCB test. Aliha et al. (2015) analyzed the stiffness of five modified asphalt mixtures and one normal mixture. The asphalt mixture results suggest that the fracture toughness is related to the modifier type, air void content, and the test temperature.

The SCB test has been successfully modeled using the FEM. Aragao and Kim (2012) developed a finite element model from the results of an SCB laboratory test. The fracture zone at the tip of the notch was monitored and processed with a digital image correlation (DIC) system. From the DIC results, a bilinear cohesive zone model was developed for the numerical simulation. Results demonstrated the rate-dependent fracture response of bituminous mixtures at a higher temperature. Elseifi et al. (2012) developed a 3D finite element model to identify the failure mechanisms and study crack propagation in the SCB test. Additionally, simulation results correlated with test results in terms of predicting the fracture performance of different asphalt mixtures. The damage in the finite element model was studied using cohesive zone elements along the notch zone. The SCB test was also used to study the fracture characteristics of dolomite rock under mixed mode. Li et al. (2013) used the scanning electron microscope to look at the damage zones of the rock material. Based on the re-mesh method of the finite element method (FEM), authors looked at five different criteria to predict the cracking path. Huang et al. (2013) employed a finite element (FE) model to obtain the fracture parameters of asphalt mixtures by using regression analysis. The SCB results from the FE model agreed with the published literature, thus, the proposed model could be used to characterize the fracture resistance of asphalt mixtures.

An extended finite-element model (XFEM) coupled with a cohesive zone model (CZM) was developed by Mahmoud et al. (2013). Authors studied seven asphalt mixtures, some of these

mixtures included recycled asphalt pavement (RAP), warm mixture asphalt (WMA), and lime and polymer-modified asphalt. The analysis of the experimental results was used to develop an FE model simulating the SCB test. The main objective of this research was to investigate the crack propagation in the SCB test and to predict SCB simulations for experimental cases with different notch depths. Results suggest that the FE model was successful in simulating the SCB test mechanism for crack propagation. Wang et al. (2013) also employed the XFEM to study Crumb rubber modified (CRM) asphalt mixtures. The investigation focused on the stress distribution during cracking, and the crack path in order to provide some insights on the fracture behavior of these type of asphalt mixtures.

Lancaster et al. (2013) studied the fracture propagation of asphalt mixtures using the XFEM. The XFEM results were compared with laboratory SCB results. It was concluded that the XFEM is a potential candidate for modeling cracking in asphalt mixtures. A more recent paper on the mixed mode fracture behavior of asphalt mixtures was given by Xie et al. (2016). The Extended Finite Element Method (XFEM) was used to understand the fracture process of the asphalt specimens. Special attention was drawn to the crack trajectory, crack initiation angle, and the onset of fracture for asphalt mixtures under mode II.

Castillo et al. (2015) analyzed the mechanical response of asphalt mixtures by using a Finite Element approach. The model size was 10 cm by 10 cm. Coarse aggregate phase and air voids were randomly generated throughout the model, therefore, different samples with different aggregate distributions can be generated. The aggregate shape and aggregate angularity were also considered in this study. Two gradations and three different air void contents were the variables in the mixture. The two gradation sizes were NMAS of 12.5 mm and 19 mm. For the air void content, 4%, 7%, and 10% were used. The number of the simulations for each case was 100, thus,

a total of 600 replicates were studied. Each simulation was subjected to tensile stress for 300 s. The research team found that as the air void content increases, the samples experienced more displacement and more critical damage area. Moreover, damage in samples with a high percentage of air voids occurred sooner than in mixtures with low content of air voids. For the effect of the aggregate size, simulations with 19 mm NMAS gradation showed higher mean vertical deformation and greater critical damage area than samples with 12.5 mm NMAS.

From the literature, the experimental SCB test has been extensively used to investigate the fracture resistance of asphalt mixtures subjected to changes in the test temperature and mixture design. From the numerical side, the SCB test has been modeled to get insights into the fracture behavior and the stress distribution in the SCB. Moreover, FE models have been used to match with real asphalt material parameters according to with laboratory test results. However, current FE models have not implemented all aggregate, air void, and mastic phases of asphalt mixtures into the SCB model. In this study, a theoretical analysis of the SCB test simulated in DEM was investigated. The variability in the size and angularity of the aggregate material was considered. Additionally, air void and mastic phases were also part of the analysis. Furthermore, the properties at the interface between mastic and aggregate were set the same as the mastic for half of the models, while for the rest of the models, the interface properties were set to twice the properties of the mastic.

The SCB test has been proven to be a suitable candidate as a cracking test due to its simple setup and easiness in preparing samples directly from the laboratory or the field. Therefore, investigating the parameters involved in the cracking process of the SCB test is essential for gaining a better understanding as to the design process of asphalt mixtures.

CHAPTER III

METHODOLOGY

The modeling of the heterogeneous Semi-Circular Bending (SCB) test using the Discrete Element Method (DEM) consists of two main parts: the generation of a homogeneous SCB model, and an appropriate capture of aggregate phase. In order to achieve this, the Particle Flow Code 2D (PFC^{2D}) software version 5.0, which implements the DEM for numerical analysis, was used. In PFC^{2D}, the model domain is the working space where all the model components are generated by the user. The size of the model domain is also set by the user and it limits the dimensions of the system since objects outside the model domain are not considered in the simulation.

The model components in PFC^{2D} are referred as bodies and these include balls, clumps, and walls. The numerical software treats balls as rigid disks with a unit thickness which can move and rotate by applying the equations of motion. These equations only require the input of the mass properties (density and radius) for balls to be solved. Clumps are composed of rigid spherical pebbles and their motion is also associated with Newton's second law. The advantage of using clumps over balls is the representation of noncircular shapes in the system. Wall bodies are manifold surfaces composed of line segments which can move and rotate about its reference point. They are used to induce loading, define boundary conditions, or also to recreate certain geometric shapes. Figure 1 shows the geometrical representation of these model components.

More details about these three types of bodies can be found in the software manual (Itasca Consulting Group, Inc. (2014)).

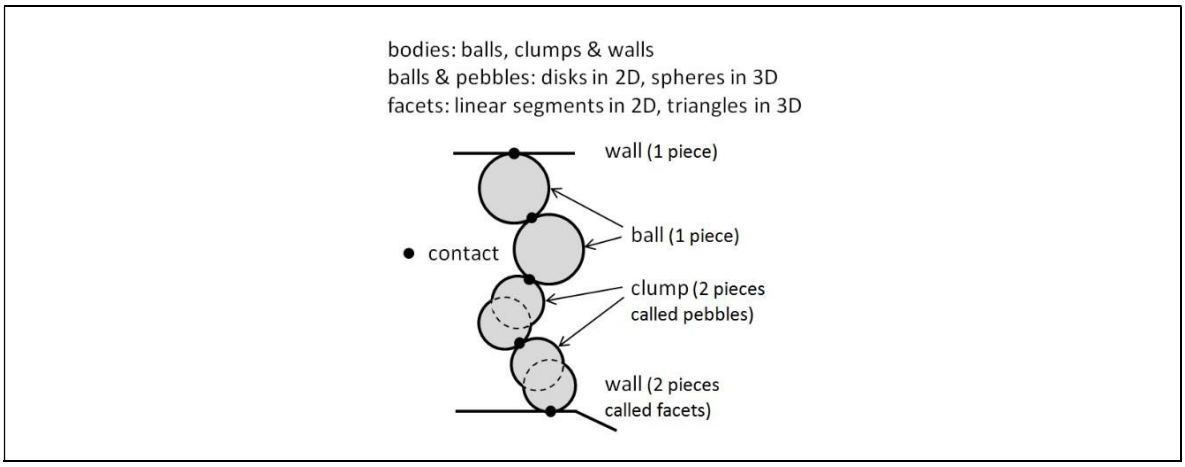

Figure 1. Particle Flow Code Software Model Components (Itasca Consulting Group, Inc. (2014))

Contact mechanics behavior between bodies can be stated in two ways. The first option is to use the already built-in contact models available in PFC, and the second option is to select the user-defined contact models where simple and complex contact behaviors can be developed. For this project, the linear contact bond model provided by PFC was used (i.e., the first option was chosen). The contact bond works as a pair of elastic springs where the normal and shear stiffnesses act at the contact point. If the normal or shear forces acting on the bonded particles is greater than the tensile or shear forces, the bond breaks. Figure 2 describes the rheological components of the linear contact bond model.

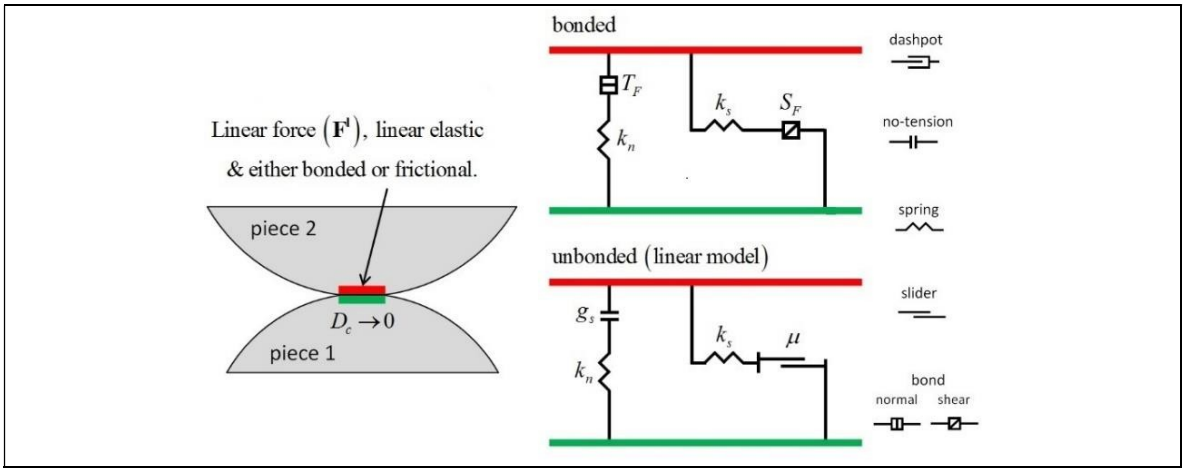

Figure 2. Rheological Components of the Linear Contact Bond Model (Itasca Consulting Group, Inc. (2014))

The time-dependent asphalt behavior in DEM is simulated by using the Burger's contact model, which uses the Kelvin and Maxwell models connected in series in the normal and shear direction. The Kelvin model combines linear springs and dashpots components acting in parallel. On the other hand, the Maxwell model incorporates the same rheological components but acting in series. Figure 3 illustrates the linear springs and dashpots components that correspond to the stiffness and viscosity parameters in both directions from the Kelvin and Maxwell models.

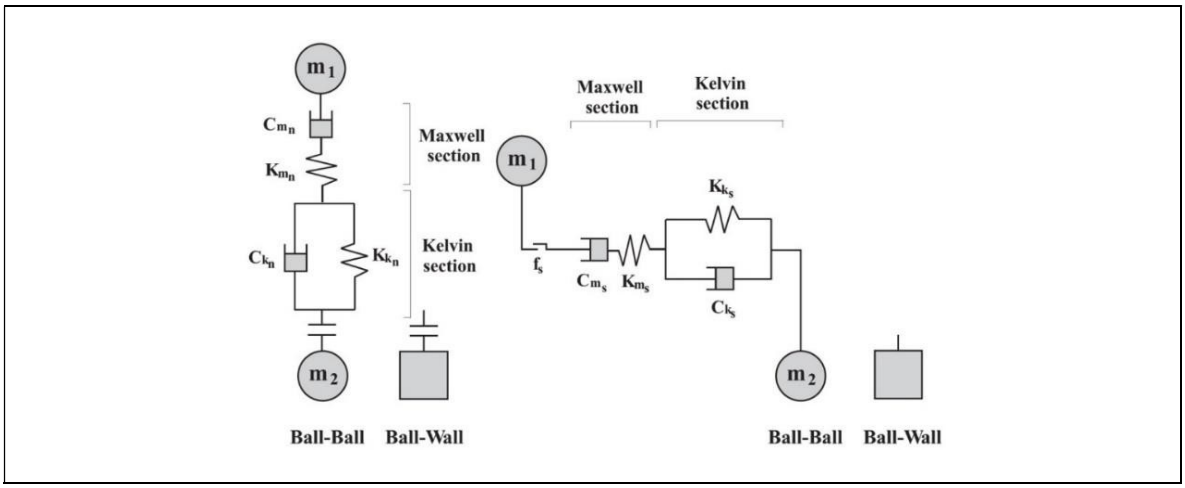

Figure 3. Rheological Components of the Burger's Model (Itasca Consulting Group, Inc. (2014))

In this project, the variability of the asphalt mixtures in the SCB test was analyzed. Parameters such as aggregate angularity, aggregate properties, air void distribution, and interface properties were included in this study. The process of generating a heterogeneous SCB model using the DEM is quite elaborate but it can be divided as follows:

- Classification of low and high angular aggregates
- Generation of aggregate clumps
- Representation of aggregate, mastic, and air void phases
- Contact properties
- Boundary conditions
- Loading model

Classification of Low and High Angular Aggregates

A goal of this project is to see the effect of the aggregate shape on the fracture behavior of asphalt mixtures. Two-Dimensional (2D) aggregate images were obtained from the Aggregate Image Measurement System (AIMS) database. The angularity index determines whether an aggregate is rounded or angular based on the aggregate's contour. After Micro-Deval (AMD) and Before Micro-Deval (BMD) aggregate images were used in this study. Masad et al. (2006) classified the angularity of AMD, BMD, and combined (AMD and BMD) aggregate images using clustering analysis. Table 1 organizes each set of images as low, medium, and high angular aggregates based on their angularity index. A combination of AMD and BMD images were used in this study. The angularity index range for low angular aggregates was from 0 to 2100. For high

angular aggregates, the angularity index range was from 2100 to 5000. Figure 4 shows the variability of the angularity index for 118 aggregate images taken from AIMS database. In this set, the aggregate shape of these samples can be categorized as rounded and subrounded; Figure 5 illustrates these aggregates. The number of samples used for high angularity aggregates was 120. Based on their shape, they are considered as subangular and angular aggregates. Figure 6 shows the angularity index for each aggregate and Figure 7 exhibits the aggregate shape for these samples.

Table 1. Angularity Classification for BMD, AMD, and Combined (after Masad et al. (2006))

	Low	Medium	High
Angularity - BMD	< 2590.26	2590.26 - 3615.90	> 3615.90
Angularity - AMD	< 1738.04	1738.04 - 2717.17	> 2717.17
Angularity - Combined	< 2056.82	2056.82 - 3193.55	> 3193.55

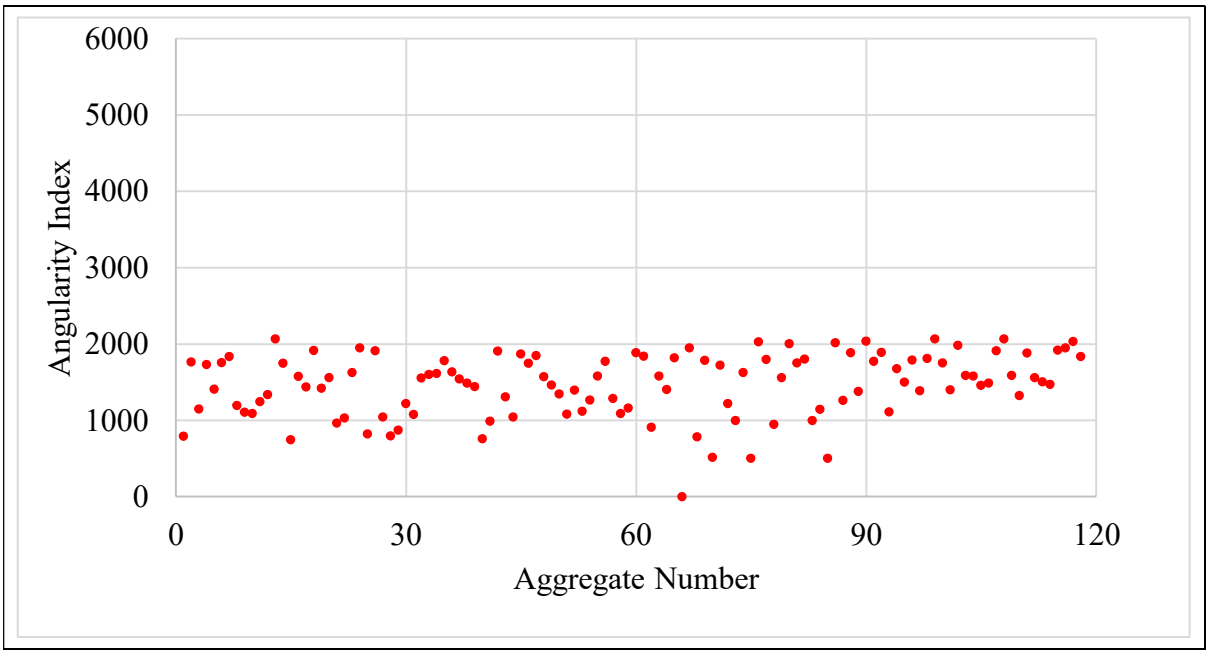

Figure 4. Angularity Index of Low-Angularity Aggregates

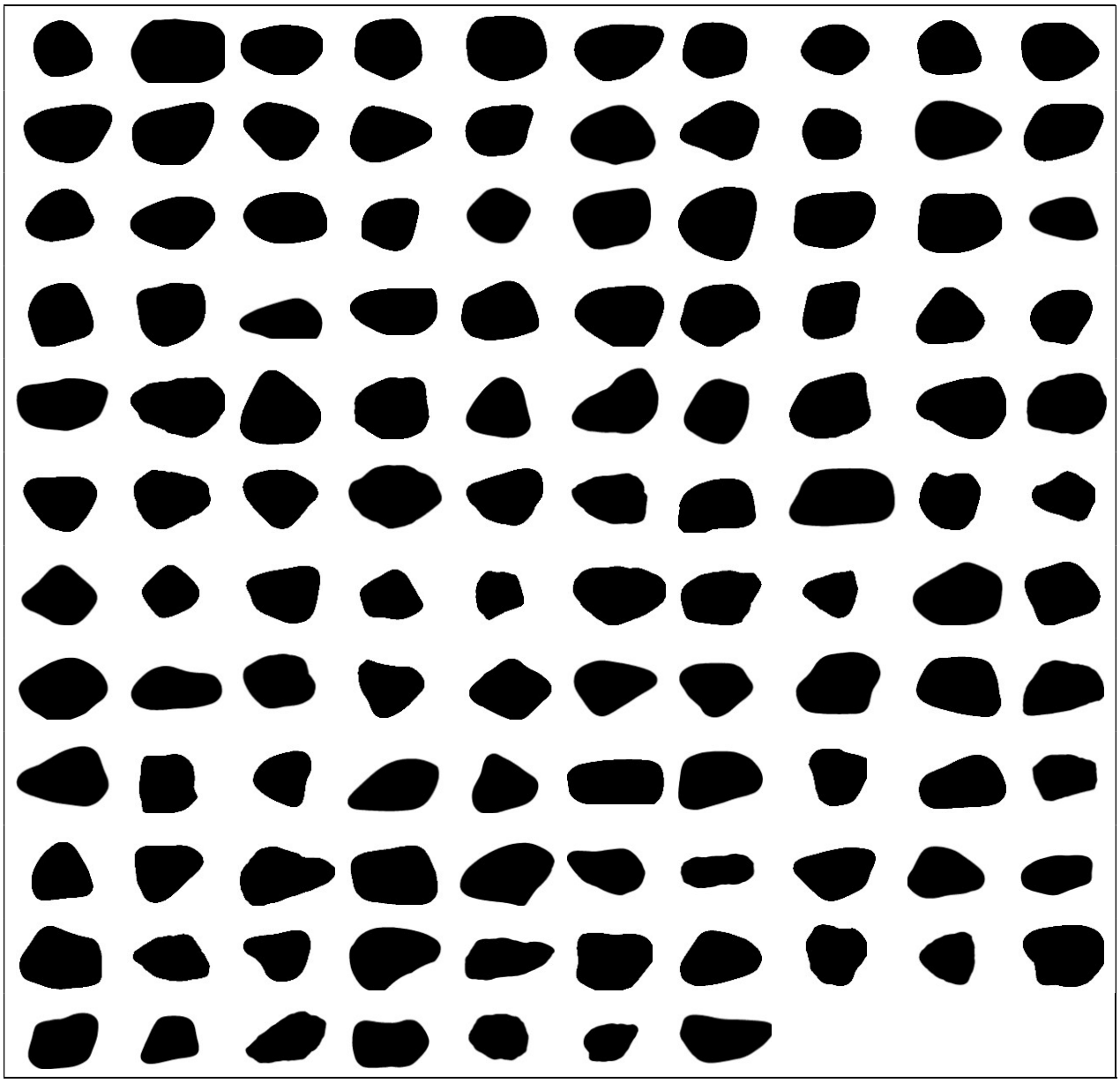

Figure 5. Low-Angularity Aggregates

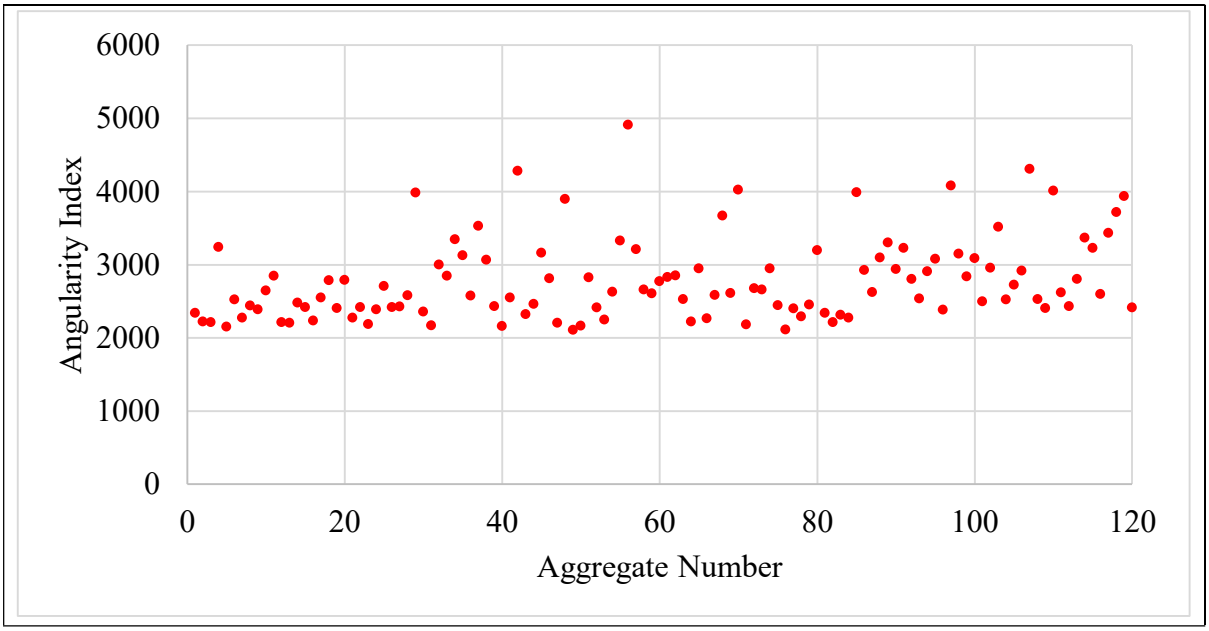

Figure 6. Angularity Index of High-Angularity Aggregates

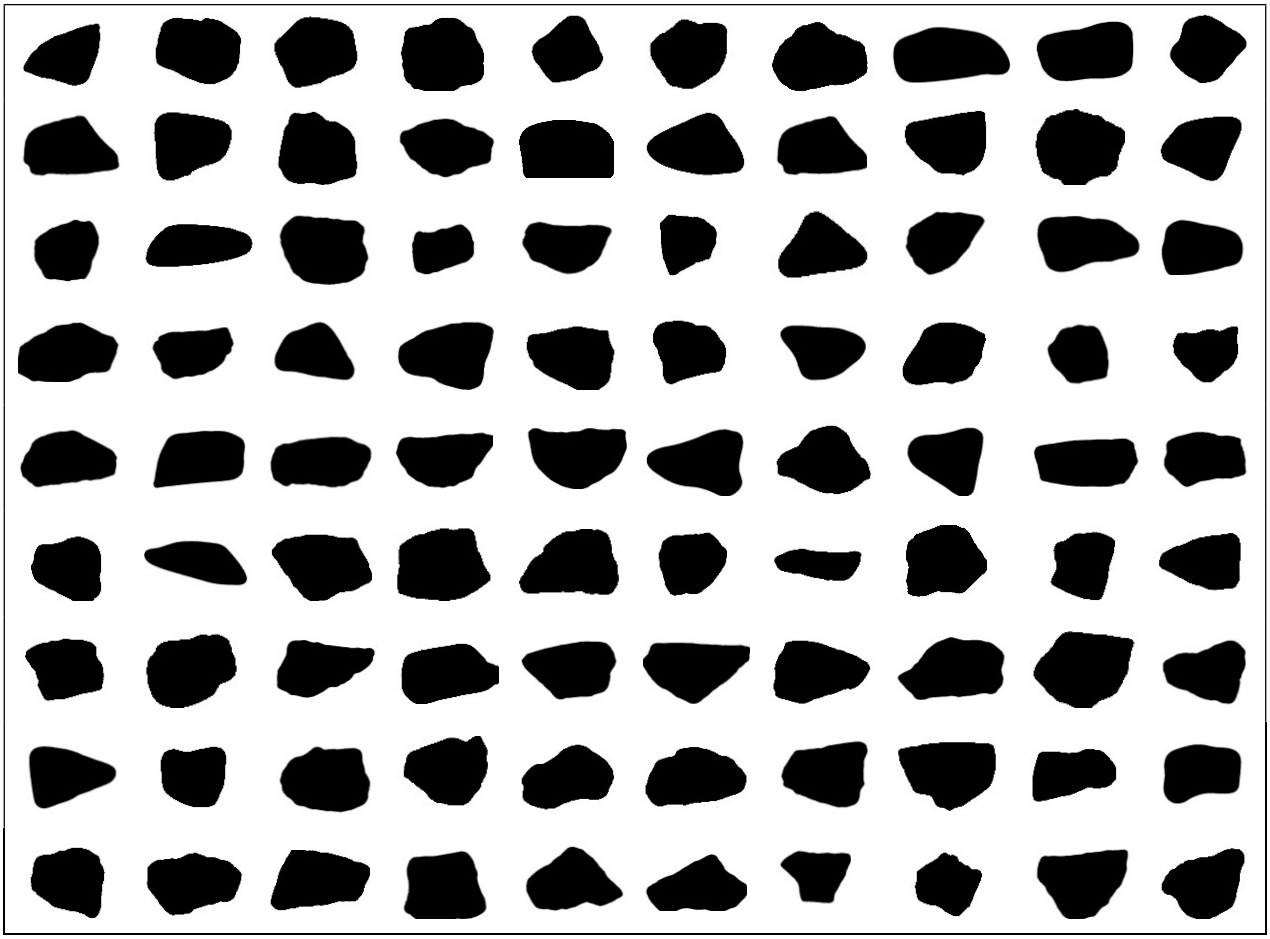

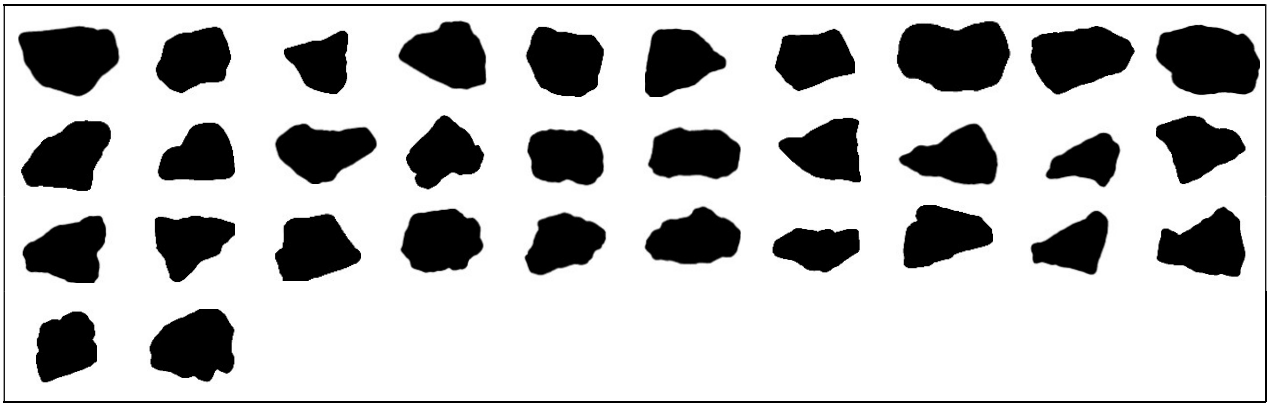

Figure 7. High-Angularity Aggregates

Generation of Aggregate Clumps

Aggregate material characterization is a fundamental part of the development of the heterogeneous SCB model. In this project, two mixtures were used: Superpave and Coarse Matrix High Binder (CMHB). The generation of aggregate clumps consisted of quantifying the volumetric relationships of asphalt mixtures and the gradation size for each mixture.

Superpave and CMHB mixtures have a different percentage of coarse aggregate material. Percentage of asphalt binder, air void content, and the particle size distribution were obtained from Alvarado et al. (2007). Volumetric parameters of hot mix asphalt (HMA) were calculated using phase diagrams. This step determines the percentage of aggregate and mastic in the SCB model. Figure 8 displays the phase diagram used to calculate the percentage of each component in the mixture.

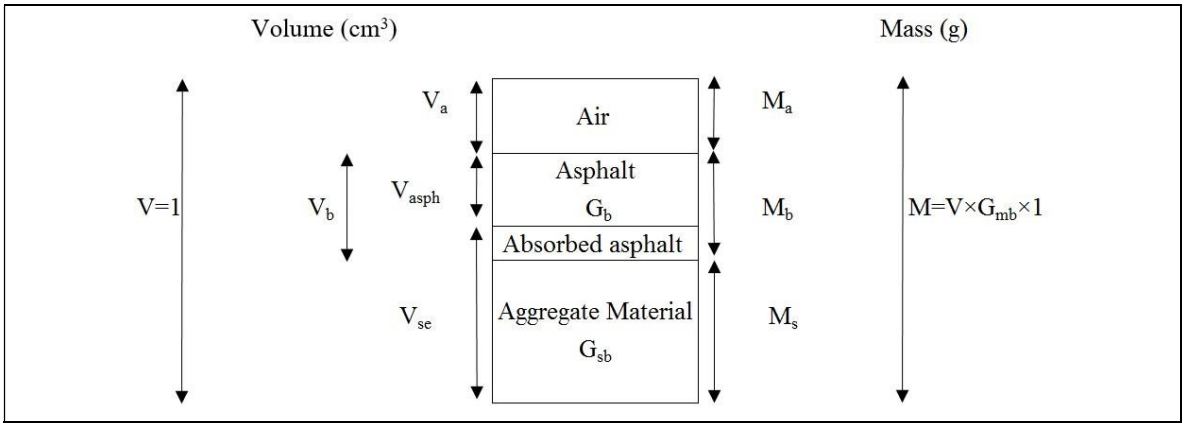

Figure 8. Volumetric Relationship of the Asphalt Mixtures

The procedure is as follows:

- Calculate bulk specific gravity of the mixture (G_{mb}) following Eq. [1]:

  Maximum Theoretical Specific Gravity $= \frac{G_{mb}}{1-\%Air\ voids}$ [1]

- Calculate the total mass (M) of the mixture.
- The mass of the binder (M_b) can easily be calculated by multiplying the percentage of asphalt in the mixture by G_{mb}.
- Calculate the mass of the aggregate (M_s) by subtracting the mass of the binder from the total mass.
- The next step is to calculate the volume of aggregates (V_{se}) using Eq. [2]

$$V_{se} = \frac{M_s}{G_{sb} \times 1.0} \quad [2]$$

- Since we know the volume of air voids, we can now easily calculate the volume of asphalt (V_{asph}) by subtracting the volume of aggregates and volume of air voids from the total volume.
- Calculate the volume of asphalt binder (V_b), using Eq. [3]

$$V_b = \frac{M_b}{G_b \times 1.0} \quad [3]$$

- Calculate the rest of the unknowns by adding or subtracting asphalt parameters.

Table 2 shows the percentage of aggregate, mastic, and air voids for each asphalt mixture. According to Alvarado et al. (2007), these asphalt combinations have the same amount of air voids based on their mixture design. CMHB – mixtures are composed of 67% of aggregate material and 28% of mastic. On the other hand, Superpave combinations show a slight difference between aggregate and mastic phases; 49% corresponds to coarse aggregate, while 46% of the mixture is considered mastic.

Table 2. Percentage of Asphalt Mixture Components

Mixture Type - Aggregate	Coarse aggregate	Mastic	Air void
Coarse Matrix High Binder - Granite	67.32%	28.68%	4%
Coarse Matrix High Binder - Hard Limestone	67.86%	28.14%	4%
Coarse Matrix High Binder - Soft Limestone	66.77%	29.23%	4%
Superpave - Granite	49.42%	46.58%	4%
Superpave - Hard limestone	49.80%	46.20%	4%
Superpave - Soft Limestone	49.14%	46.86%	4%

The next step is to calculate the gradation size based on the volumetric relationships of asphalt mixtures. In the field, sieve analysis consists of the distribution of granular material through sieves. Each sieve is placed on top of one another according to its opening size. The sieve with the largest opening size will be placed at the top, while the sieve with the smallest opening size will be at the bottom. Table 3 lists the gradation test results for the two mixtures taken from Alvarado et al. (2007). This shows how much aggregate material was retained at a certain sieve as a percent of the total weight before passing to the next sieve.

Table 3. Gradation Test for CMHB and Superpave Mixtures

Sieve #	Sieve size (mm)	% Retained	
		Coarse Matrix High Binder	Superpave
	25.40	0	0
	19.05	1	1
	12.70	21	4
	9.53	19	3
4	4.75	23	15
8	2.36	16	35
16	1.19	6	13

In this project, coarse aggregate retained up to No. 8 sieve were generated in PFC^{2D}. The modeling of aggregates smaller than 2.36 mm causes major delays in the simulations and produces unexpected results. To reduce delay, a new gradation system was needed where No. 16 sieve aggregate was ignored. Table 4 summarizes the modified sieve analysis for CMHB and Superpave mixtures, where the grain material distribution was based only up to No. 8 sieve.

Table 4. New Gradation Test for CMHB and Superpave Mixtures

Sieve #	Sieve size (mm)	% Retained		Area of the opening (mm^2)
		Coarse Matrix High Binder	Superpave	
	25.40	0	0	506.71
	19.05	1	2	285.02
	12.70	26	7	126.68
	9.53	24	4	71.26
4	4.75	29	26	17.72
8	2.36	20	61	4.37
16	1.19	0	0	-

The modeling approach for each aggregate is based on the diameter of the opening hole for each sieve. Therefore, a single ball having the same diameter as that of the opening hole will be considered as one aggregate element for that certain sieve. The area of each circle for each sieve was used to generate several noncircular aggregates which were classified as aggregates with high and low angularity according to their angularity index.

After calculating all these parameters; the outline of each 2D aggregate image was drawn in Rhino CAD software. In PFC^{2D} aggregate drawings were identified as geometries, these were used to generate clumps that represented the aggregate phase in the SCB; Figure 9 shows this process. The clump shape is based on the geometry imported in PFC^{2D} and the software gives the user the ability to control its surface area. In this way, the area of each clump (aggregate) will correspond to the opening size of a certain sieve. The number of clumps created in the model will be based on the total area of aggregates depending on the selected mixture gradation (refer to Table 2). Air voids generated for each mixture will also depend on the percentage of air voids in each gradation. Both CMHB and Superpave mixtures consist of 4% of air voids. For this study, an air void was modeled as a disk with 1 mm in diameter in accordance with CastelBlanco (2004). The air void shape was assumed to be circular; thus, air voids were generated straight from the numerical program as clumps.

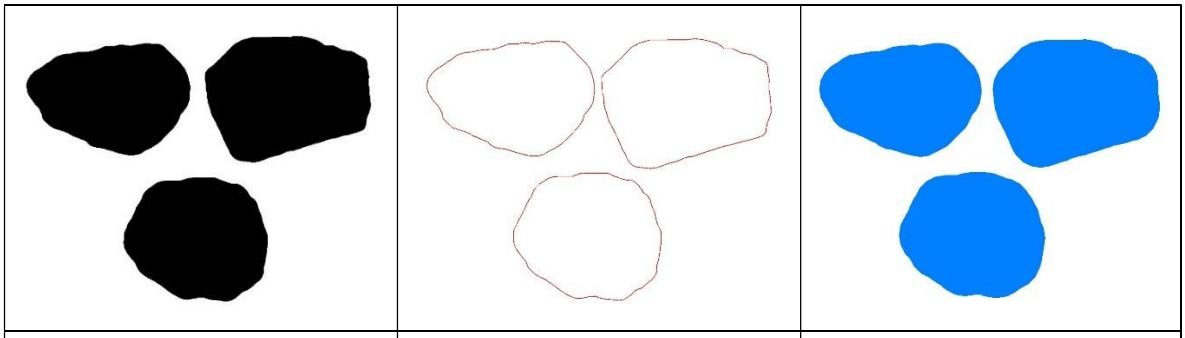

(a) (b) (c)

Figure 9. Aggregate Generation: (a) 2D Aggregate Images; (b) Aggregate Geometries; (c) Aggregates as Clumps

It is important to emphasize that the correct procedure for generating coarse aggregate phase and air voids should be in the following order:

- Generation of aggregates.
    - From largest opening sieve to smallest.

- Generation of air voids.

Otherwise, the generation of smaller aggregates first, restricts the area of the SCB for the larger aggregates. Following the procedure described above ensures that all aggregates and air voids could fit in the SCB model. PFC^{2D} generates non-overlapping clumps in which their positions are drawn from uniform distributions throughout the model domain. As a result, every time a new sample has been created, the location of clumps (aggregates) will be different from the previous sample. Figure 10 shows two CMHB samples where aggregates and air voids were randomly generated. Also, two samples were randomly generated for Superpave mixtures; this can be seen in Figure 11. In both samples for CMHB and Superpave mixtures, the percentage of aggregate and air voids was in accordance with Table 1.

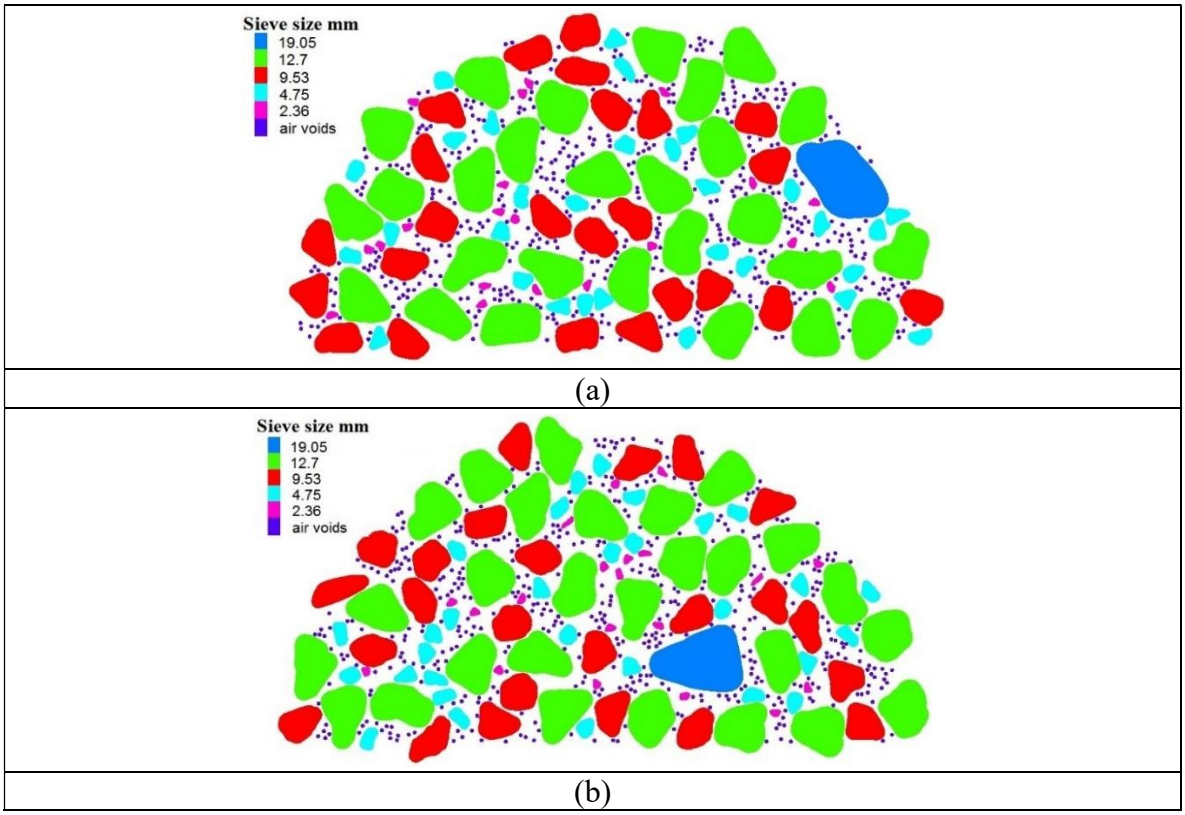

Figure 10. CMHB Aggregate Generation: (a) Sample 1; (b) Sample 2

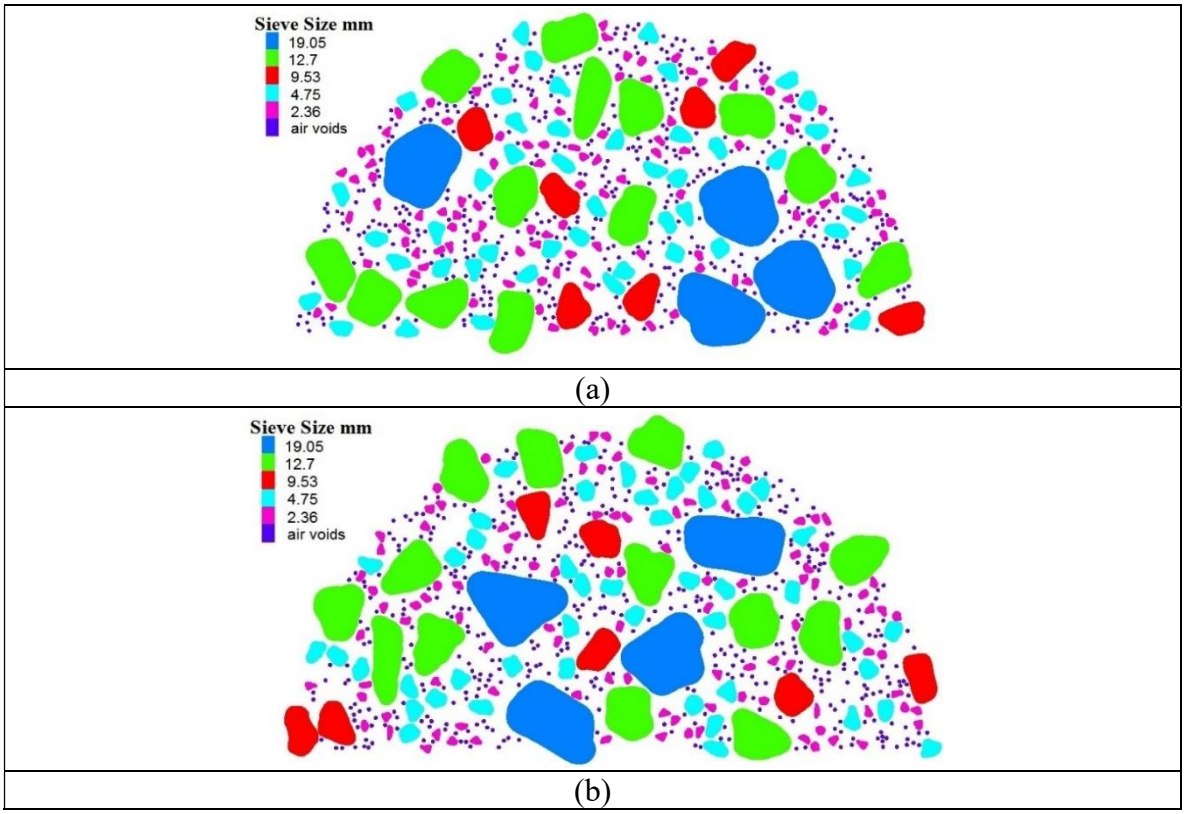

Figure 11. Superpave Aggregate Generation: (a) Sample 1; (b) Sample 2

Representation of Aggregate, Mastic, and Air Void Phases

The first part of representing the material phases of asphalt mixtures was the generation of a homogeneous SCB sample. The recreation of the SCB shape in PFC^{2D} cannot be generated from a single command line. Therefore, a circle and a rectangle were generated from the available set of predefined geometries in the software by invoking simple command lines. Both geometries were created at the origin of the model domain. The radius of the circle geometry was set to 75 mm. The rectangle geometry was used to simulate the notch in the SCB; its dimensions were 2 mm wide and 30 mm long. A plane wall was added at the origin of the model domain to divide the circle geometry into two parts, Figure 12(a) shows this scheme.

Boundary conditions were introduced to avoid particles flying around the model domain. The latter was achieved by replacing the circle and rectangle geometries with walls. Two walls were created and positioned based on the geometries already modeled to form two closed systems that were separated by the plane wall in the middle. In this context, the area of the SCB was enclosed by three different walls. From this point, only the area above the plane wall will be shown, Figure 12(b).

The next step was to generate discrete elements inside the SCB shape. There are three ways to generate balls in PFC^{2D}. The first option is to create single particles where the user can specify their location and size. The second approach is adjusting the distribution of overlapping balls to match a certain size distribution. The user can use this method from a simple command line and must specify the target porosity for the software to automatically stop when this criterion is met. The porosity in the numerical software is a ratio of total void area to total area. The last method consists of generating a collection of non-overlapping balls. In the last two methods, the user specifies the range of the ball radii and assigns the space in the model where these particles will be placed. For this project, the second method was used with a target porosity of 0.1, and the ball radii ranging from 0.2 to 0.6 mm in order to produce a random dense packing system. Figure 12(c) shows the overlapped balls in the SCB. The system was then set to an equilibrium state to reduce overlaps and dissipate energy as the balls rearrange over the SCB area. Walls and geometries were deleted, and the final state of the model is shown in Figure 13(a). Figure 13(b) shows the particle arrangement around the notch of the SCB.

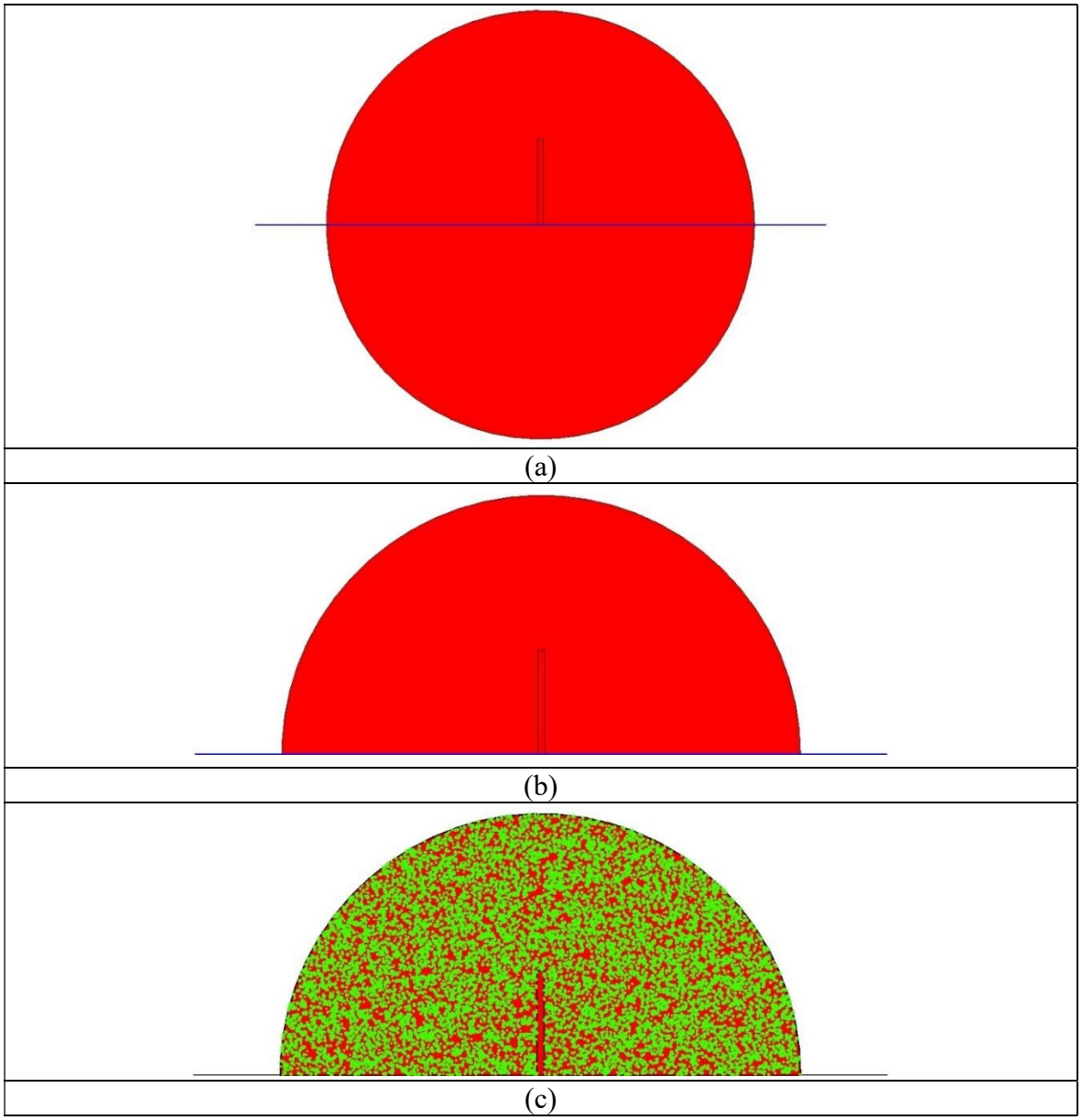

Figure 12. Generation of the SCB Model: (a) Geometries and Wall Plane; (b) SCB Enclosed Area; (c) Generation of Overlapped Balls

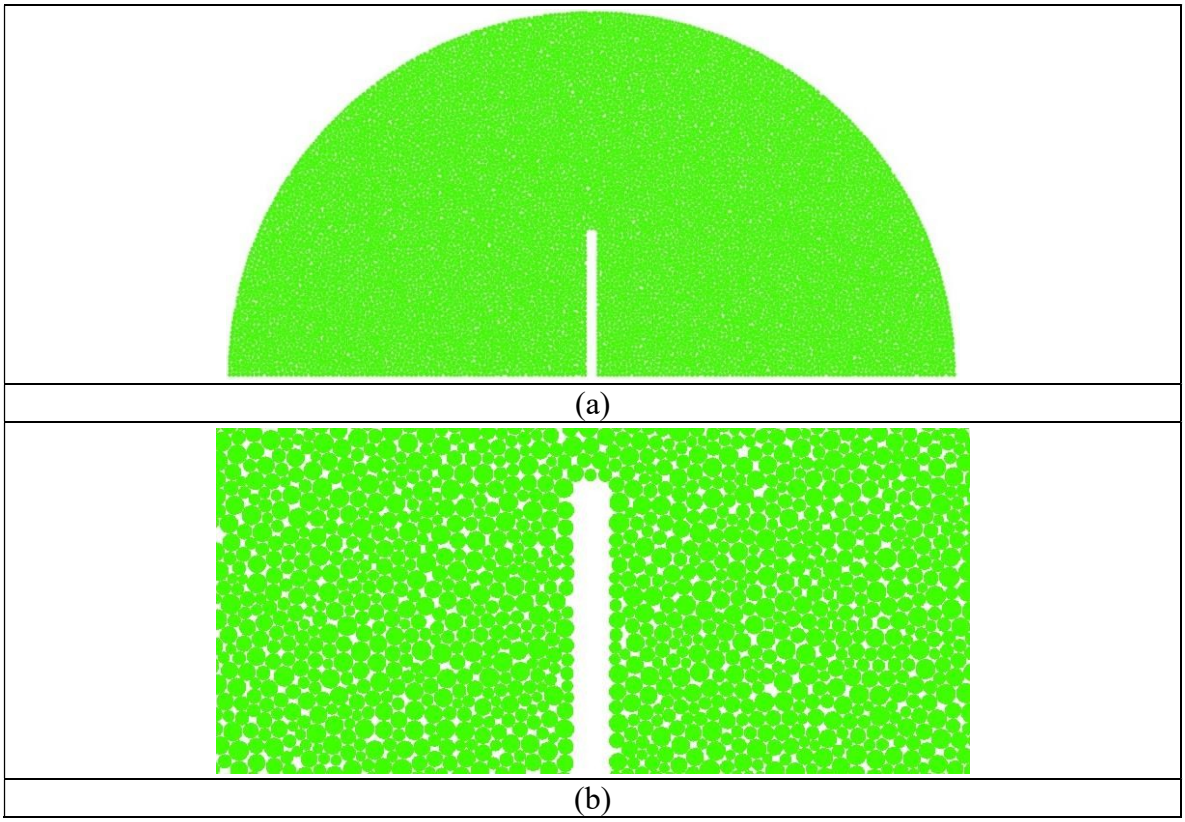

Figure 13. SCB Model: (a) Final State of the SCB; (b) Close View of the SCB Notch

The final part of this section was to import the generated clumps as geometries into the homogeneous SCB model. The aggregate phase will form based on the area of each clump (aggregate), discrete elements occupying the same area will be labeled as aggregates. In this context, large aggregates will require more balls than smaller aggregates to represent their shape. The procedure for generating air voids in the homogeneous SCB model was the same as for the coarse aggregate material. Air void clumps were imported as geometries into the homogenous assembly of balls. Discrete elements representing the air void content were deleted from the model in order to represent real test conditions. Figure 14 shows the final state for both mixtures gradation samples.

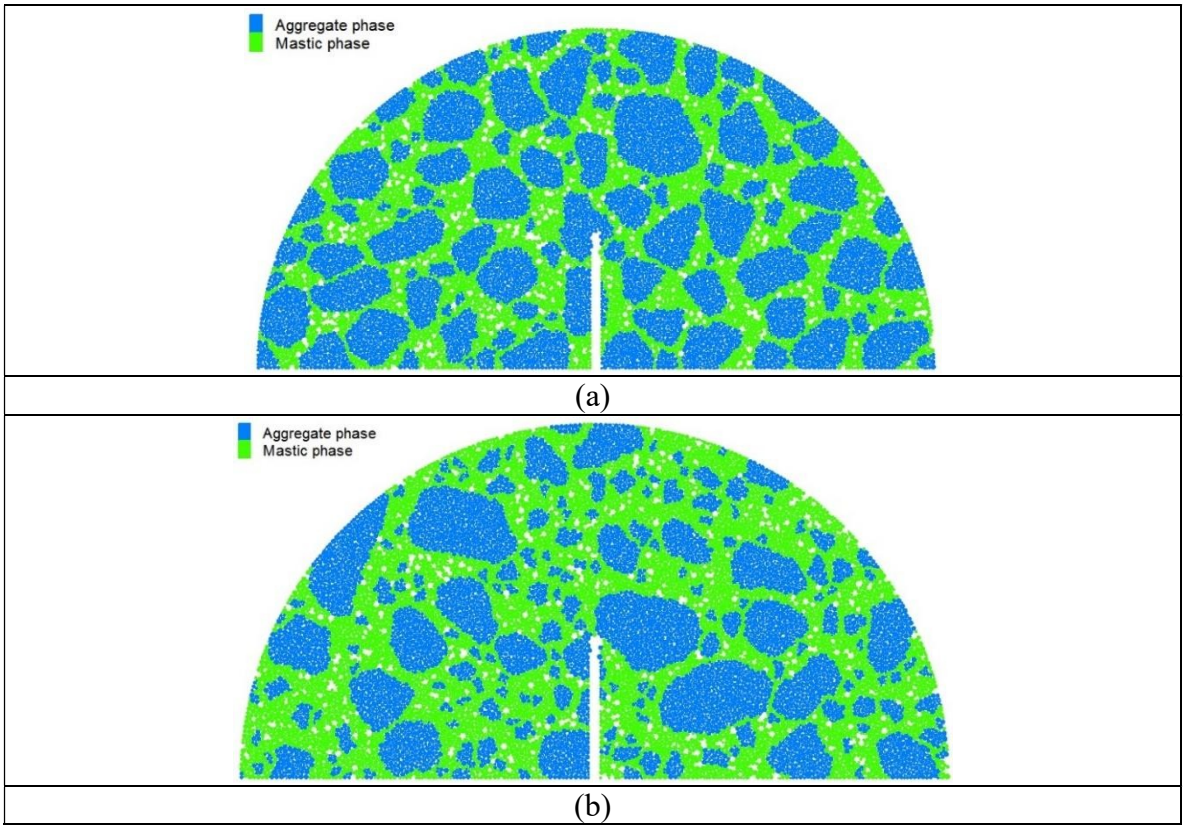

Figure 14. Heterogeneous SCB Model: (a) CMHB Mixture; (b) Superpave Mixture

Contact Properties

The compression strength, tensile strength, and modulus of elasticity properties of the aggregate material were taken from Alvarado et al. (2007). Cylindrical rock specimens with 5.8 cm in diameter and 5 cm height were tested. These samples were extracted from masses retrieved from quarries. The tensile and compression strength were determined using the splitting tensile test and the compression test machines, respectively. The calculation of the material's stiffness was obtained from nondestructive testing (NTD) techniques, including seismic and ultrasonic methods.

Aggregate calibration tests were performed in PFC^{2D} to determine the numerical aggregate properties. It is important to point out that, for these tests, the linear contact bond

model was used. The splitting tensile test was represented with a circular vertical cross-section model. On the other hand, the compressive test machine was simulated in the numerical software with a rectangular cross-section of the laboratory specimen. Dimensions from the laboratory testing were the same as for the experimental testing. Force was applied at the top and bottom of both samples by generating wall bodies.

The first step in the calibration process was matching the experimental aggregate stiffness using a high bond strength value to prevent particle breakage. Then, the normal and shear bond strengths were adjusted until the compressive and indirect tensile numerical values matched the experimental parameters. Figure 15 shows the aggregate calibration for the compressive strength, tensile strength, and aggregate stiffness.

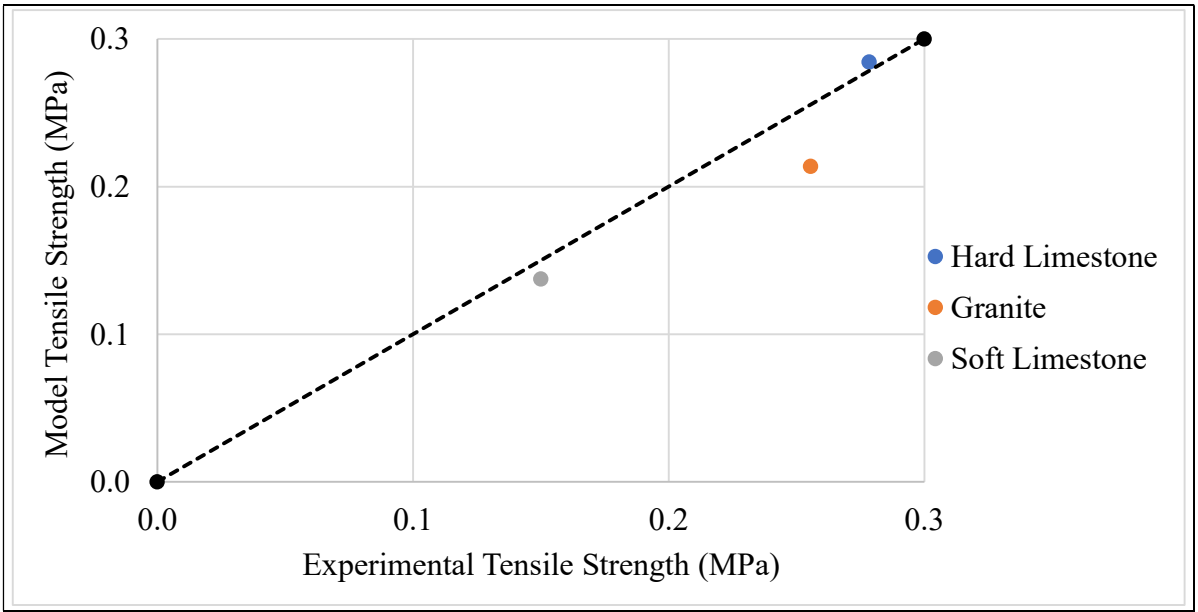

(a)

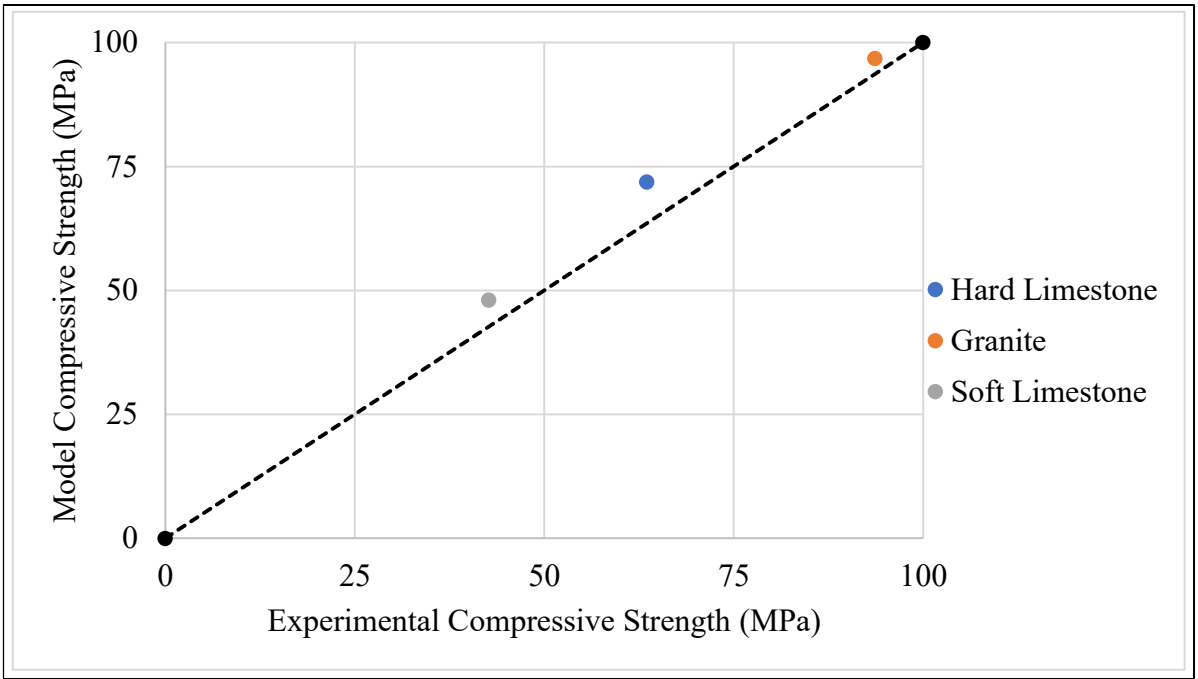

(b)

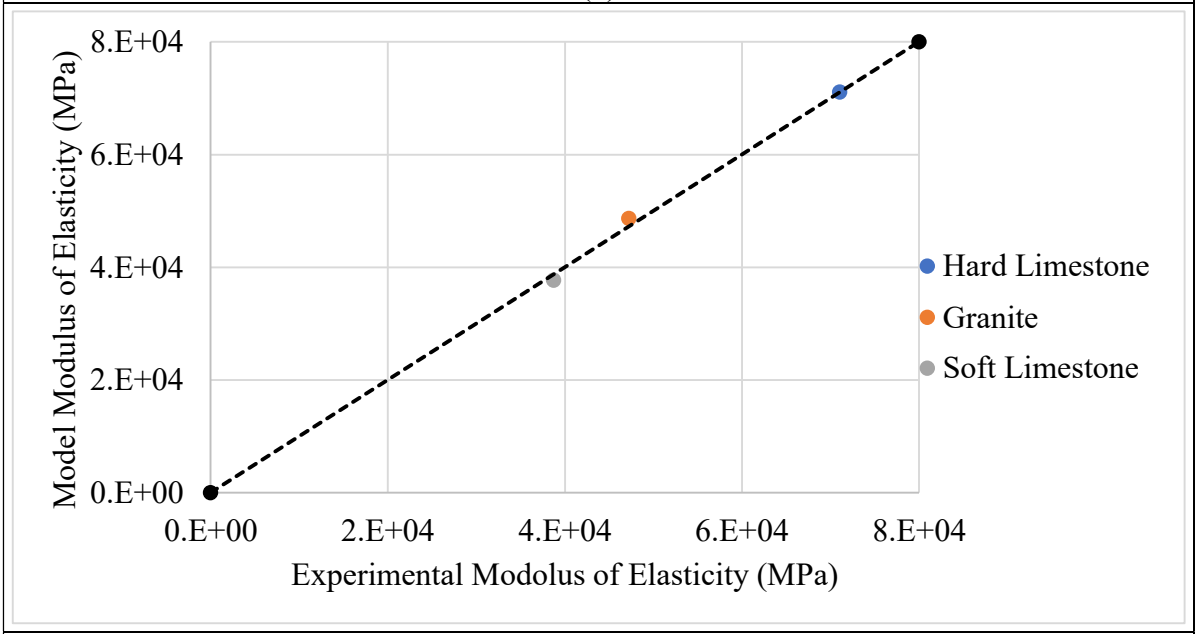

(c)

Figure 15. Aggregate Calibration Tests: (a) Tensile Strength; (b) Compressive Strength; (c) Modulus of Elasticity

The numerical aggregate properties were used to perform the calibration of the asphalt mixtures. To do this, the indirect tensile test was simulated in PFC^{2D}. The asphalt mixtures characterization was obtained from X-ray images. The modeling of the X-ray images into the

numerical software involved a MATLAB™ routine to successfully recreate the aggregate and mastic phases. The numerical model dimensions were the same from the 2D asphalt mixture images. Figure 16 shows the Superpave and CMHB mixtures modeled to conduct the indirect tensile test in PFC^{2D}. The main goal for conducting the indirect tensile test was to get the linear contact bond properties for the mastic phase. Table 5 summarizes the experimental and modeling results for the asphalt mixtures.

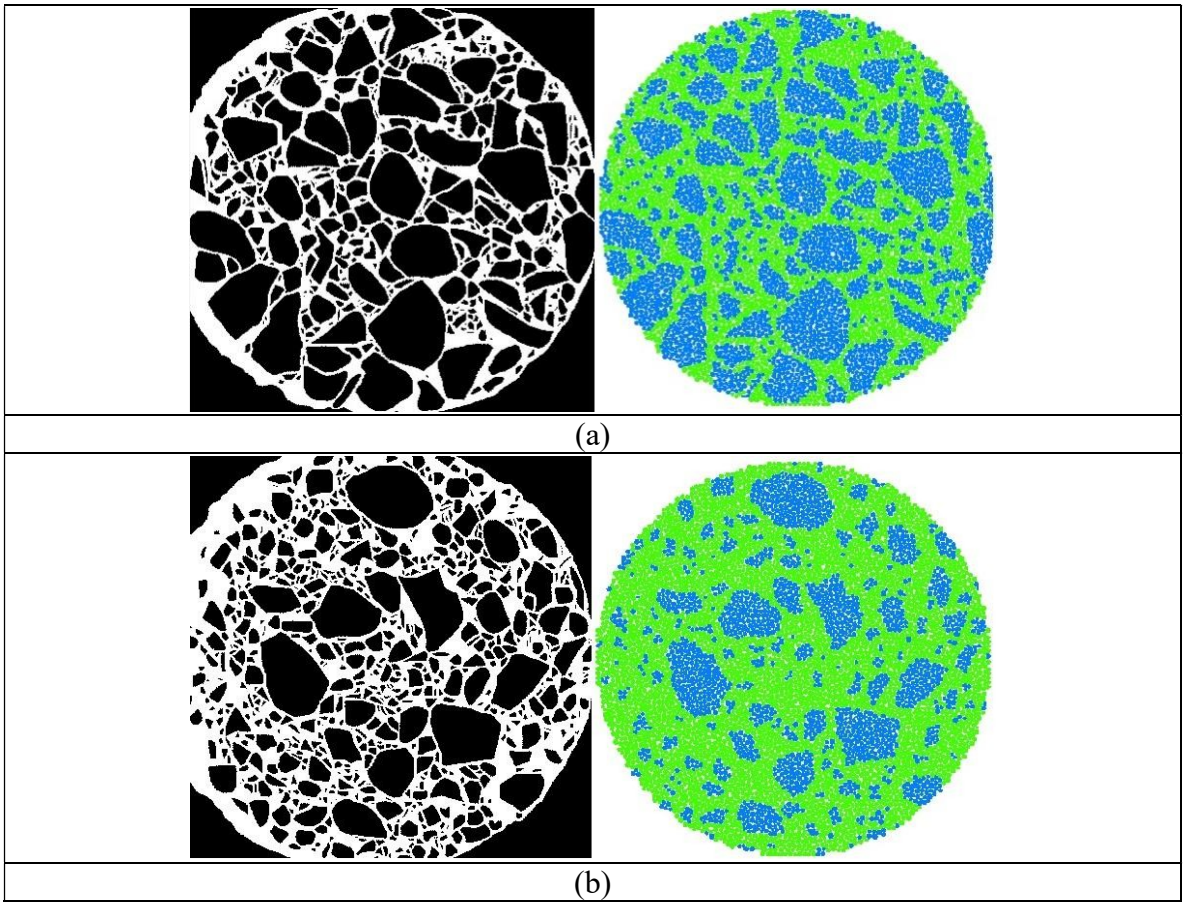

Figure 16. Internal Structure of Asphalt Mixtures: (a) CMHB; (b) Superpave

Table 5. Comparison of Experimental and Modeling Results of Asphalt Mixtures

Mixture	Aggregate Type	Experimental Values		DEM Values		% Error	
		Max Force (N)	Displacement (m)	Max Force (N)	Displacement (m)	Max Force	Displacement
CMHB	Hard Limestone	5778	0.00135	5711	0.00139	1.16	2.93
	Granite	4622	0.00151	4667	0.00149	0.96	1.00
	Soft Limestone	5225	0.00156	5134	0.00158	1.75	1.11
Superpave	Hard Limestone	6702	0.00082	6983	0.000849	4.20	3.63
	Granite	6484	0.00136	6580	0.001324	1.49	2.48
	Soft Limestone	6947	0.00103	6766	0.001062	2.61	3.00

Table 6 contains the final matrix of the asphalt mixtures generated with the total number of simulations for each case. In order to study the effect of the interface strength on the fracture resistance of asphalt mixtures, two approaches were followed. The first method was to set the interface properties the same as the mastic-mastic contact, whereas, for the second method, the properties of the interface were set as twice those of the mastic.

Table 6. Asphalt Mixtures Generated to Study the Variability of the SCB

Mixture	Angularity Index	Interface property	# of simulations
Granite - CMHB	> 2100	mastic – mastic	100
		twice the mastic	100
	< 2100	mastic – mastic	100
		twice the mastic	100
Hard limestone -CMHB	> 2100	mastic – mastic	100
		Twice the mastic	100
	< 2100	mastic – mastic	100
		Twice the mastic	100
Soft limestone - CMHB	> 2100	mastic – mastic	100
		Twice the mastic	100
	< 2100	mastic – mastic	100
		Twice the mastic	100
Granite – Superpave	> 2100	mastic – mastic	100
		Twice the mastic	100

	< 2100	mastic – mastic	100
		Twice the mastic	100
Hard limestone – Superpave	> 2100	mastic – mastic	100
		Twice the mastic	100
	< 2100	mastic – mastic	100
		Twice the mastic	100
Soft limestone – Superpave	> 2100	mastic – mastic	100
		Twice the mastic	100
	< 2100	mastic – mastic	100
		Twice the mastic	100

Boundary Conditions

The supports were located 12.5 mm apart from both edges. This distance has been the standard when performing the SCB test, thus, boundary conditions were introduced within the model as fixed balls at the distance previously mentioned. Figure 17 shows the SCB model with the supports located at the bottom of the sample.

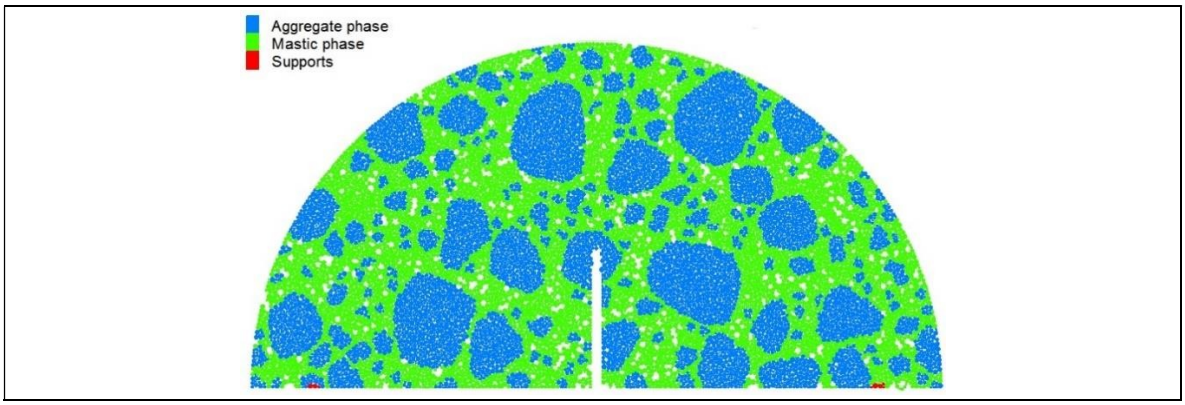

Figure 17. SCB Model with Supports

Loading

Cai et al. (2014) described the importance of determining an optimum loading rate to maintain accuracy in the simulation. Therefore, a wall speed study was conducted in order to determine the speed of the loading wall. Figure 18 contains the different loading speeds attempted in the SCB model. The results of peak force for loading speeds slower than 1 mm/s

were similar. However, as the loading speed decreases, the computational time increases. Therefore, it was determined that the optimum speed of the wall should be 0.5 mm/s.

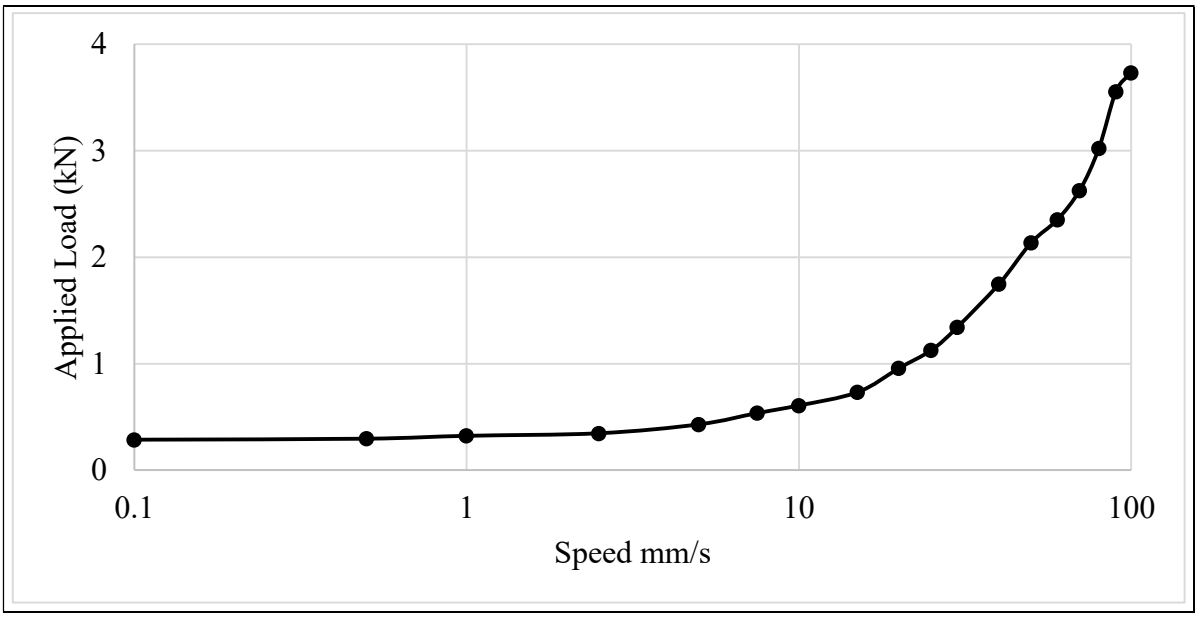

Figure 18. Wall Speed Study (Loading Speeds are in Log Scale)

Following the steps described above, the asphalt mixtures phases can be represented in the SCB model, aggregate and mastic properties can be given for each phase separately, and loading conditions are properly set to get accurate results from the simulation. The procedure for testing each mixture – case is simple. First, the internal structure of the SCB is generated based on the two angularity sets. Second, two separate data files which control the contact property at the interface and the properties of the aggregate and mastic are used. This is to differentiate between the simulations with modified interface properties. Third, after assigning material properties, another data file adds a wall body into the model to induce loading. Since the total number of simulations is 100 for each mixture – case, a python script which is embedded in PFC^{2D} is used to automatically give properties and induce loading for each of the simulations for each mixture – case.

CHAPTER IV

RESULTS AND DISCUSSION

This study introduces a theoretical performance analysis of the Semi-Circular Bending (SCB) test using the Discrete Element Method (DEM). The variability of the SCB test was studied using two aggregate mixtures gradation. For each mixture, two angularity aggregate indexes, three different aggregate types, and two contact properties at the interface between aggregate and mastic were used. A total of 100 simulations were generated for each mixture case; thus, 1200 specimens were considered for Coarse Matrix High Binder (CMHB) and Superpave mixtures.

In the numerical software, every aggregate generated in the model was set to a specific code-number according to its angularity index. For each simulation, each aggregate code-number was imported to MATLAB™ to calculate the average angularity index for that mixture-angularity case. Figure 19(a) illustrates the average angularity index for CMHB mixture with high angularity aggregates. While Figure 19(b) shows the average angularity index for CMHB mixture with low angularity aggregates. Both cases show the variability of having a wide range of particle angularity indexes available to choose from in the program.

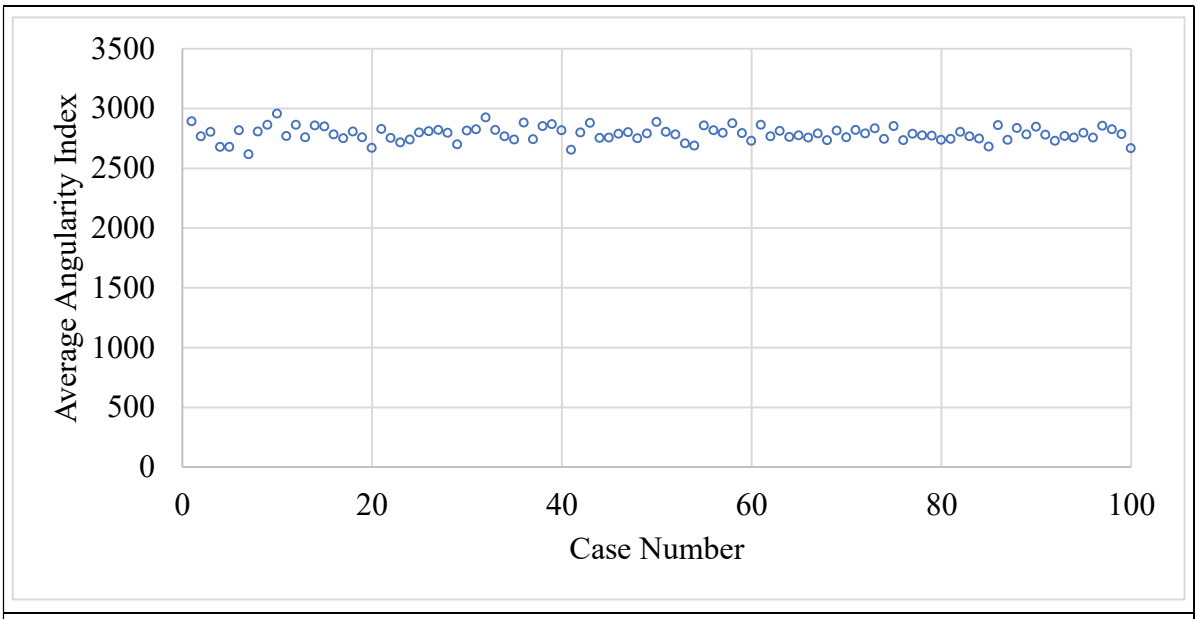

(a)

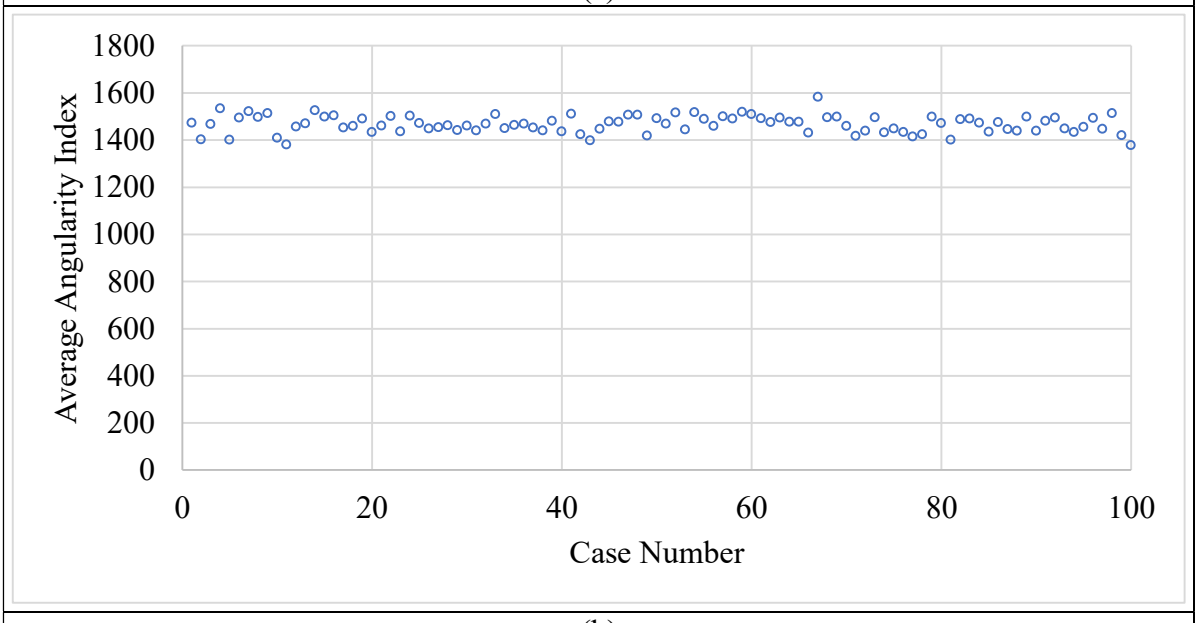

(b)

Figure 19. CMHB Mixture Simulations: (a) High Angularity Index; (b) Low Angularity Index

Two cases were randomly selected to better illustrate the variability of the aggregate angularity within the model. Figure 20(a) shows a CMHB mixture case with high angularity

index. For the same mixture, Figure 20(b) presents the aggregates generated in the model with low angularity index. Both graphs proved that the random-generator technique from the numerical software provided acceptable results in terms of selecting random particles from the two angularity sets available.

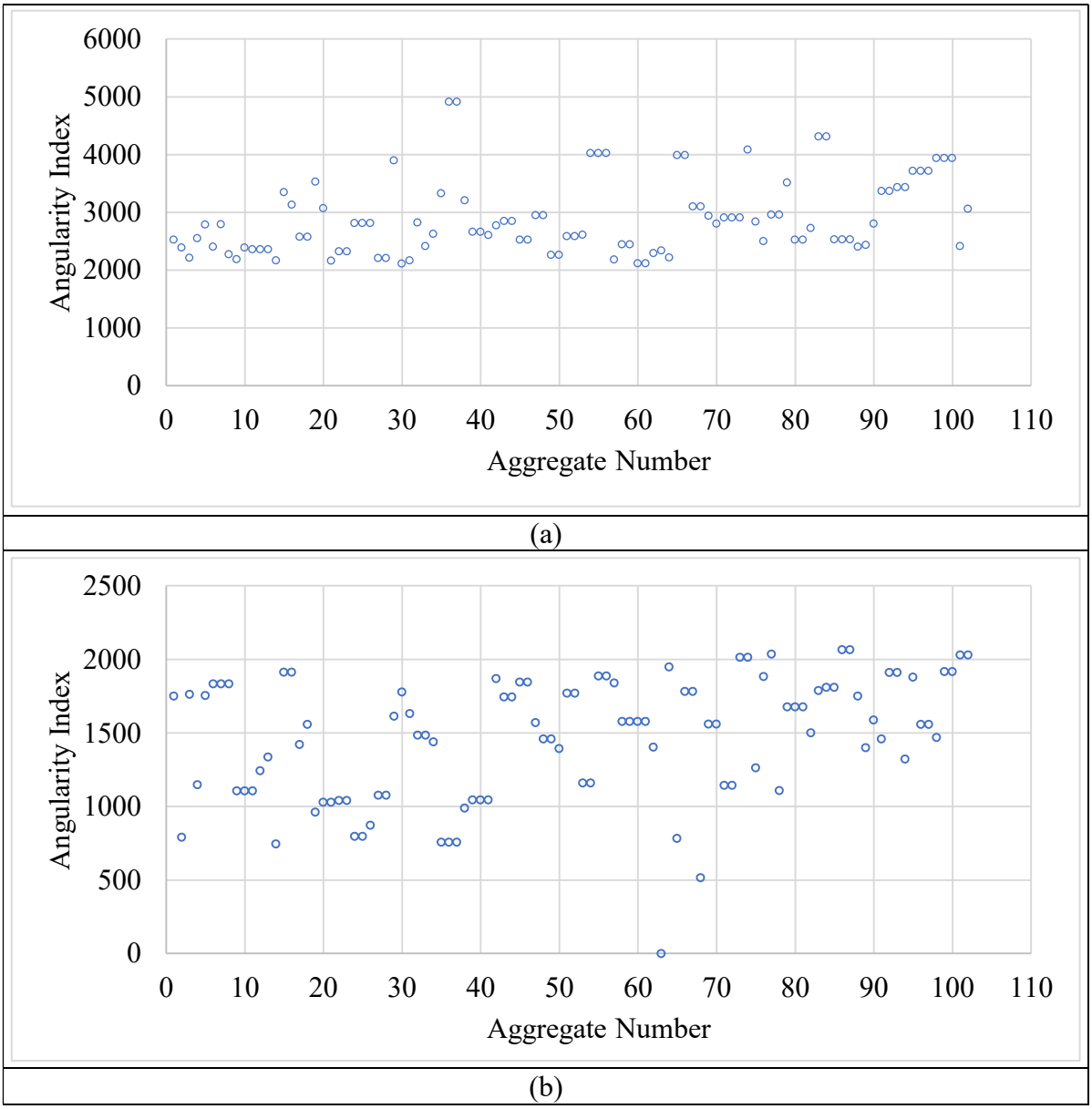

Figure 20. Variability of Aggregate Angularity in CMHB Mixtures: (a) High Angularity; (b) Low Angularity

The variability for Superpave mixtures with high and low angularity index are shown in Figure 21(a) and Figure 21(b), respectively. The range of the average angularity index for Superpave mixtures – high angularity was from 2500 to 3000. On the other hand, the range of the average angularity for Superpave simulations with low angularity was from 1400 to 1600.

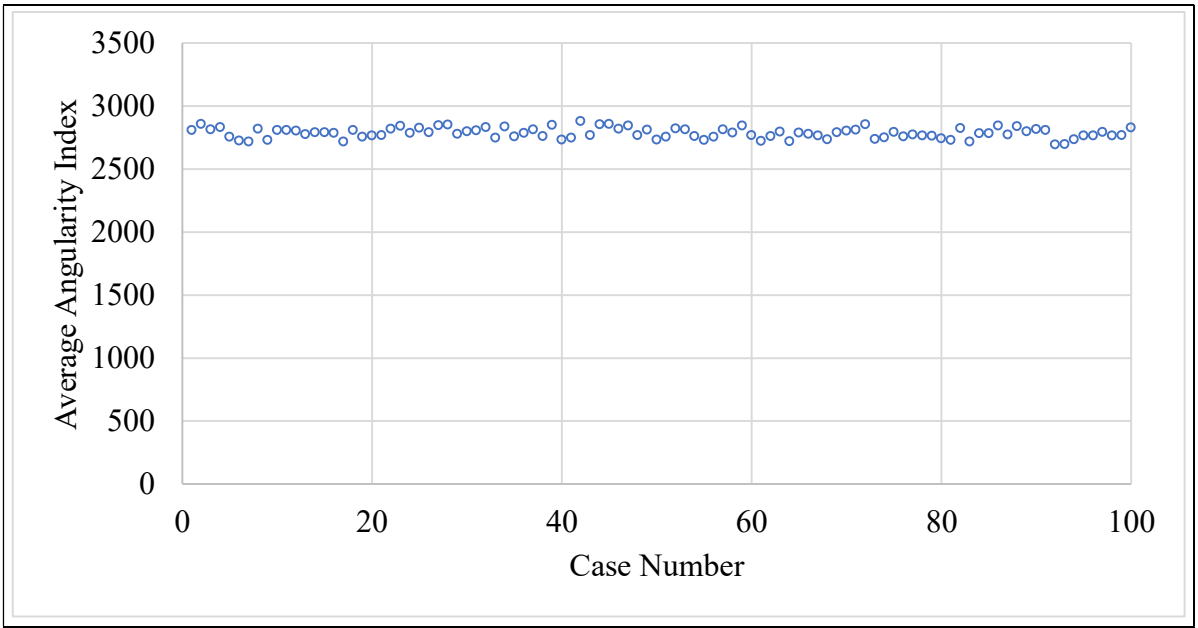

(a)

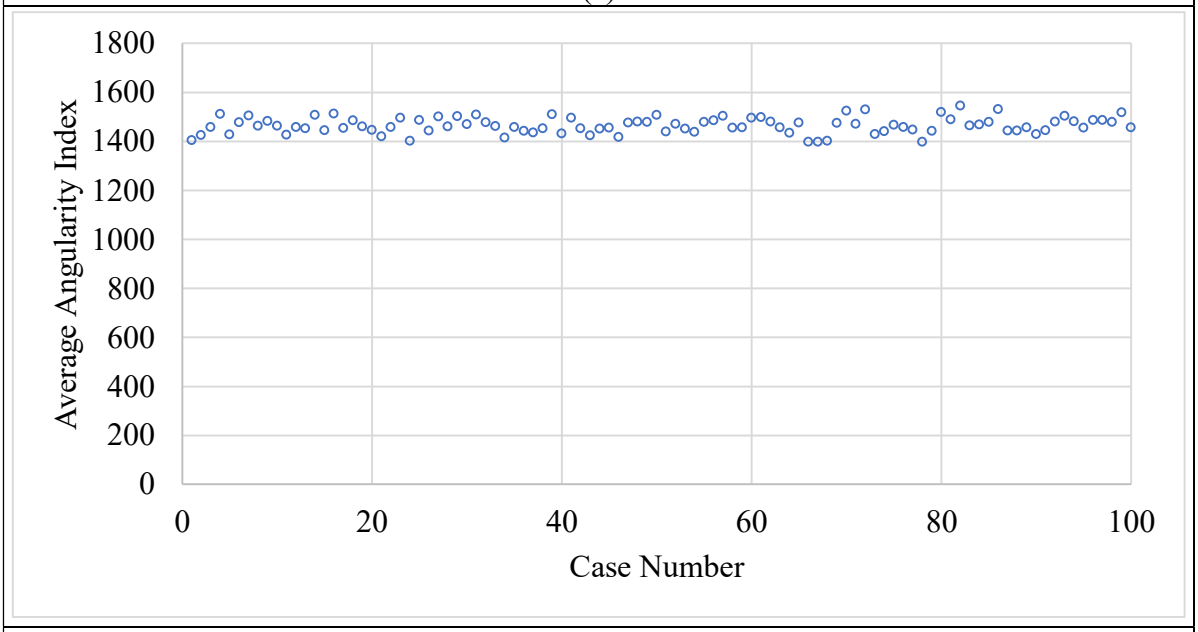

(b)

Figure 21. Superpave Mixture Simulations: (a) High Angularity Index; (b) Low Angularity Index

Again, two random samples from the Superpave mixture were selected to show the variability of the aggregate angularity. Figure 22(a) corresponds to the variability of the Superpave mixture with high angularity aggregates. Figure 22(b) shows the total number of aggregates generated with low angularity. The random generation of the aggregate material in the model is well depicted in both graphs and demonstrates the potential of the numerical software to recreate the generation of asphalt mixtures as is the case in real laboratory conditions.

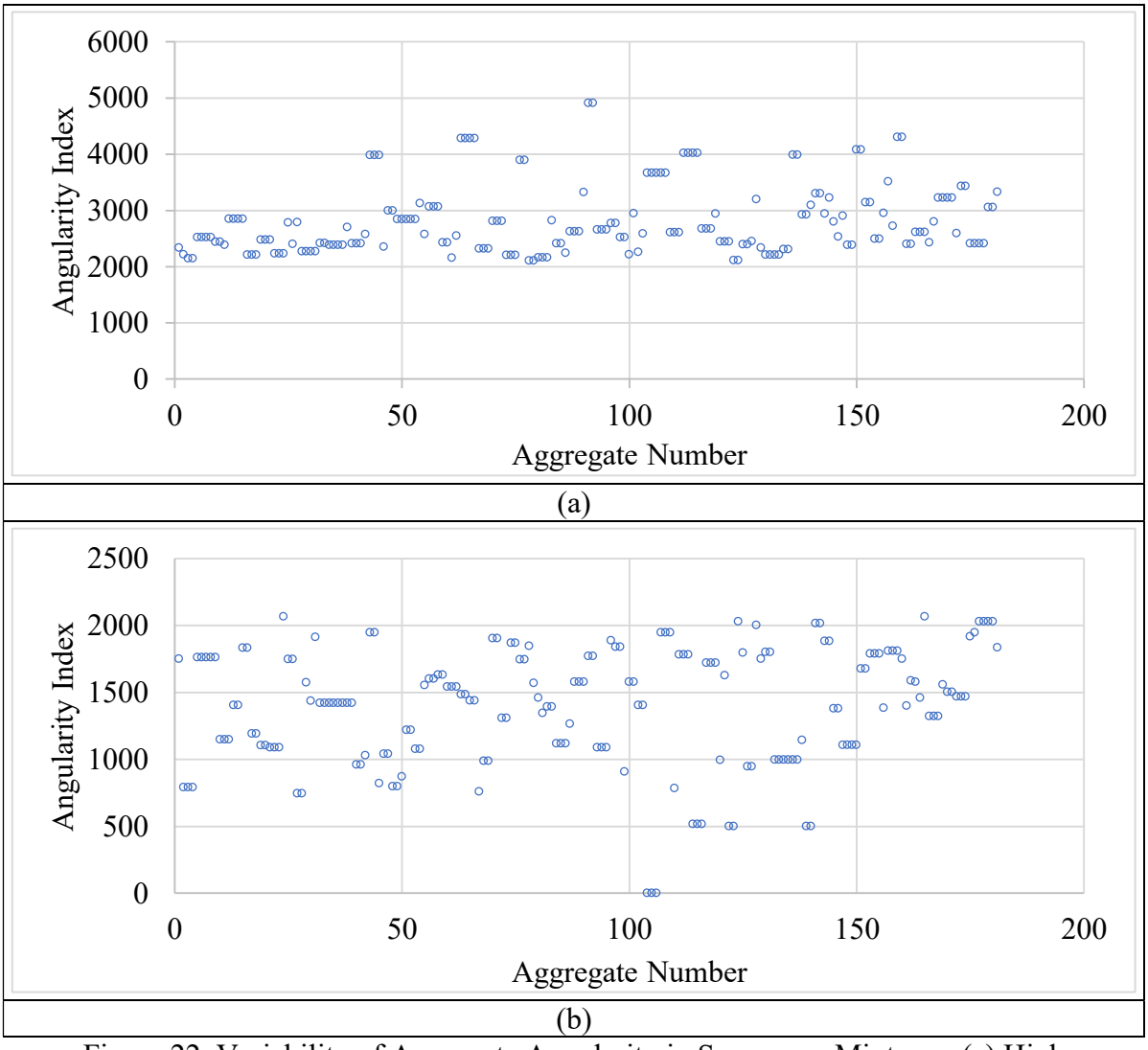

Figure 22. Variability of Aggregate Angularity in Superpave Mixtures: (a) High Angularity; (b) Low angularity

Simulation Results with Interface Properties Mastic-Mastic

The following examples consist of having the properties at the interface between mastic and aggregate the same as mastic. Figure 23 shows all asphalt mixture combinations arranged based on the angularity index. Therefore, Superpave and CMHB simulations were grouped together with respect to their angularity index to examine the simulations that produced the highest and lowest peak forces.

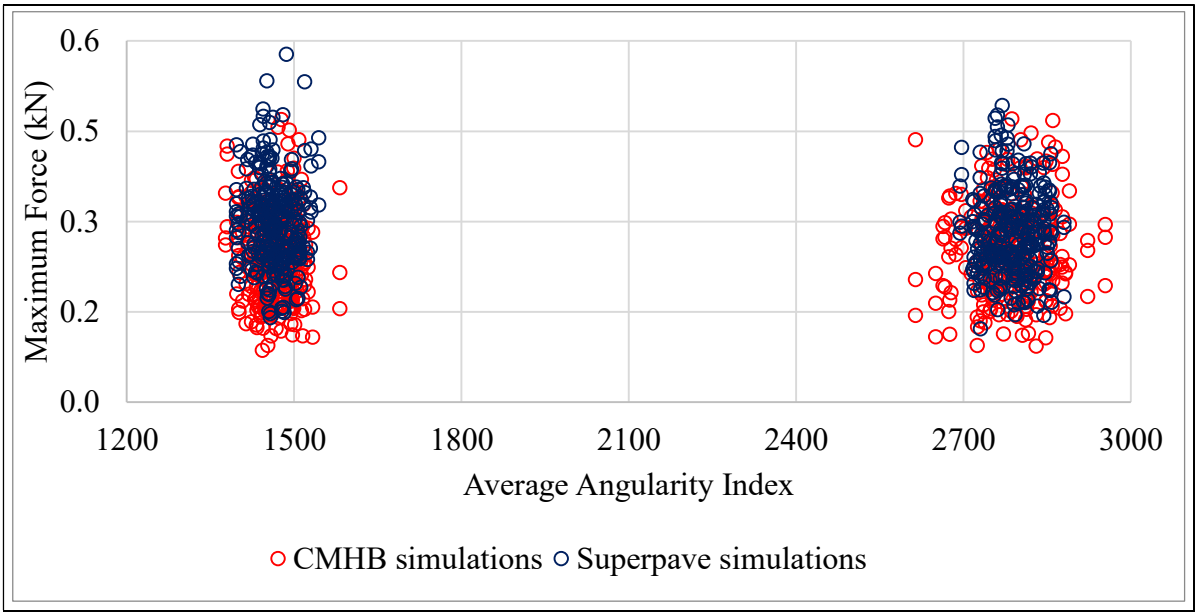

Figure 23. Superpave and CMHB Simulations

Figure 24 illustrates all the asphalt mixtures simulations with high angularity index. To avoid constant repetition, the following examples will include high aggregate angularity index. The range of the maximum force was between 0.1 and 0.5 kN, and the average angularity index was between 2600 and 3000.

As explained in the beginning of this section, one model with a certain average angularity index was used in different cases to include the three aggregate properties. The three cases circled in green in Figure 24 are shown in Figure 25. These were CMHB specimens. The crack path

from these samples was very different for each sample and affected their performance differently as well.

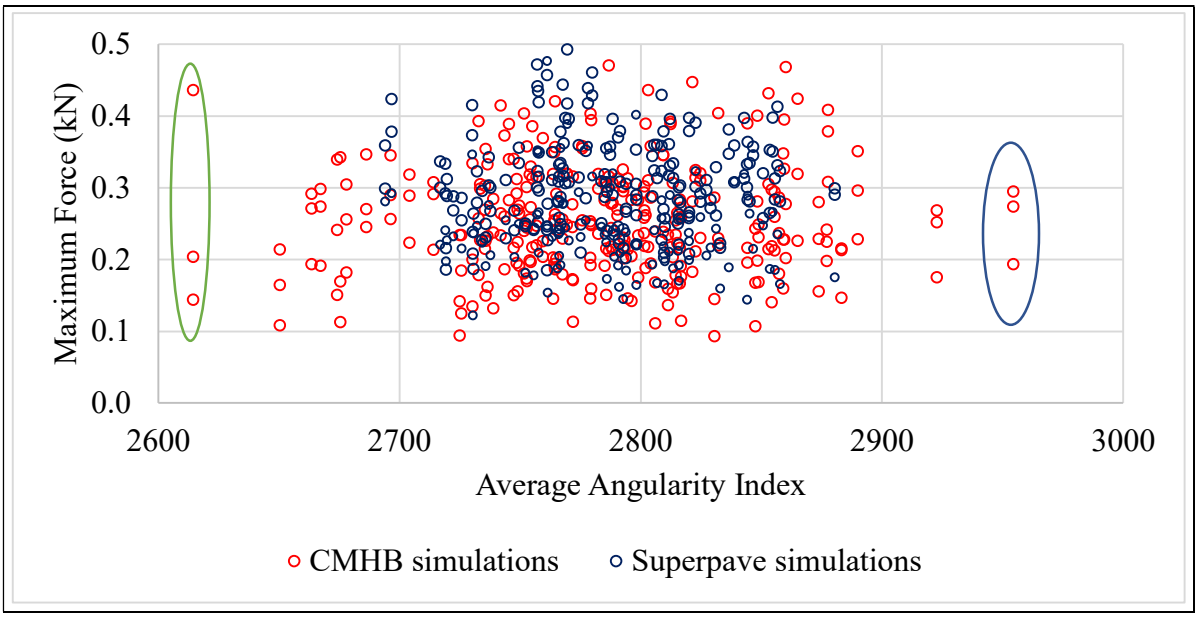

Figure 24. CMHB and Superpave Simulations – High Aggregate Angularity

Based on the SCB test configuration, the crack initiation should start at the tip of the notch and continue all the way up until total failure occurs. In the first two samples of Figure 25, the crack initiated at the tip of the notch and continued its way up in the mastic phase by going around the aggregate material. Additionally, cracks tend to develop through air voids rather than going only in pure mastic phase. Moreover, both cracks showed the same path but the crack in CMHB – hard limestone mixture was longer than CMHB – granite, Figure 25(b) and Figure 25(a), respectively. The contact bond of the mastic for CMHB – hard limestone is stronger and this could be the reason why it sustained more load. The maximum peak force recorded for CMHB – hard limestone and CMHB – granite was 0.203 and 0.143 kN, respectively.

The crack path for CMHB – soft limestone was completely different from the other two cases. The crack developed not only in the mastic but also in the aggregate phase. Hence, this

case showed the maximum peak force recorded from these three samples, which was 0.436 kN. The same behavior exhibited by these three samples was also seen in the three specimens circled in blue in Figure 24.

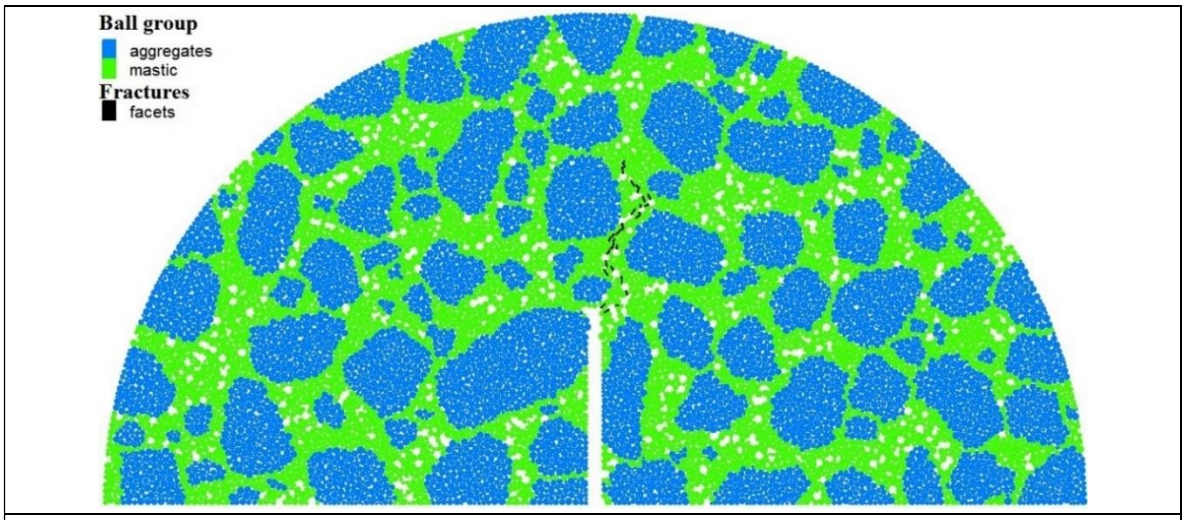

(a)

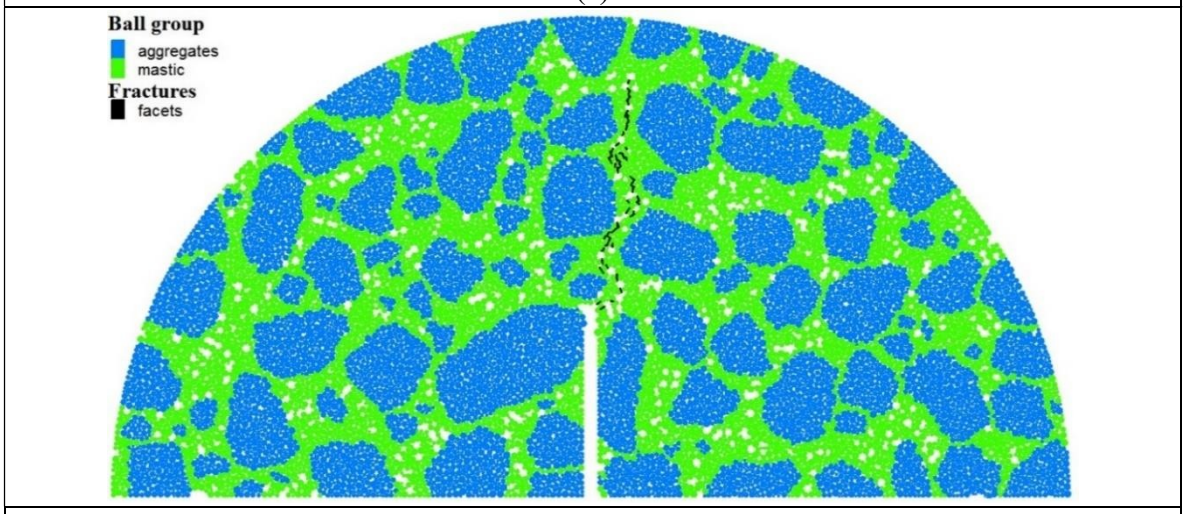

(b)

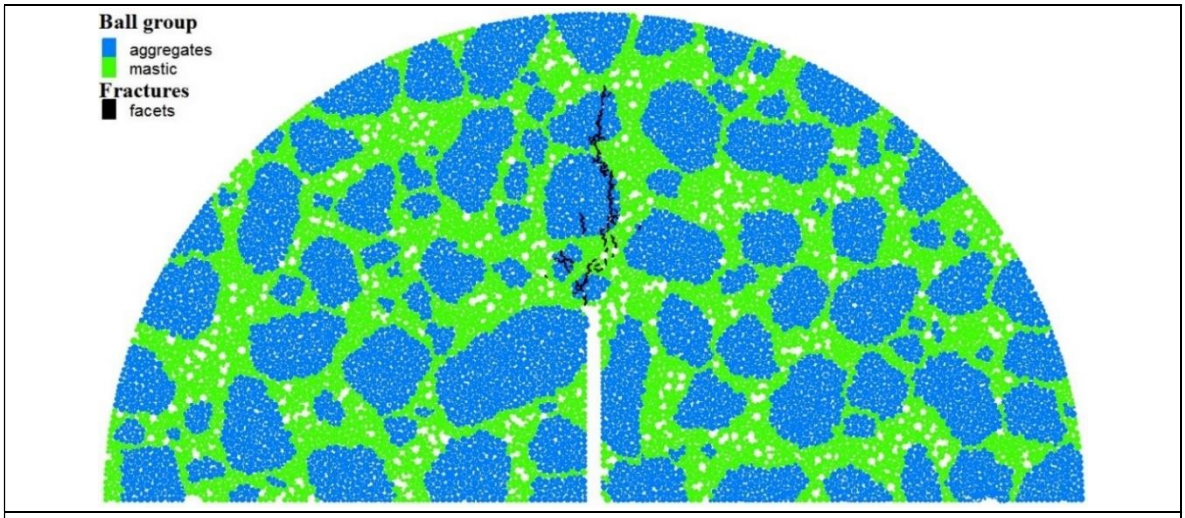

(c)

Figure 25. CMHB Samples - Aggregate Property: (a) Granite; (b) Hard Limestone; (c) Soft Limestone

One of the lowest peak forces recorded was found in the CMHB – granite combination. Figure 26 shows that cracking started at the tip of the notch and developed in the mastic region. As the crack was advancing between two aggregate particles, it got stuck at the interface (aggregate and mastic). The force – displacement graph shown in Figure 27 exhibits that the stiffness of the model increases when this happened.

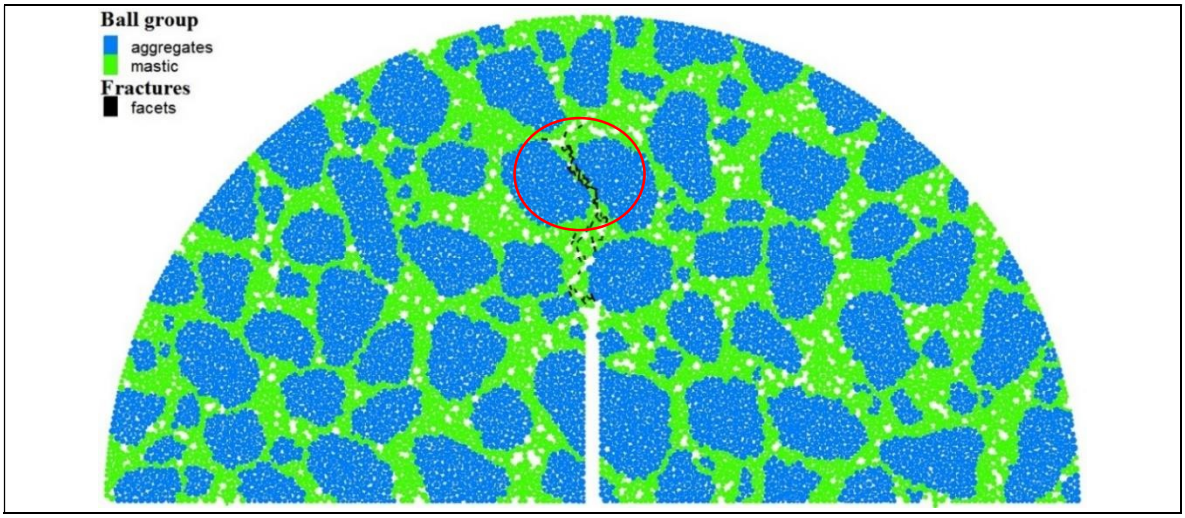

Figure 26. Cracking in CMHB – Granite Sample

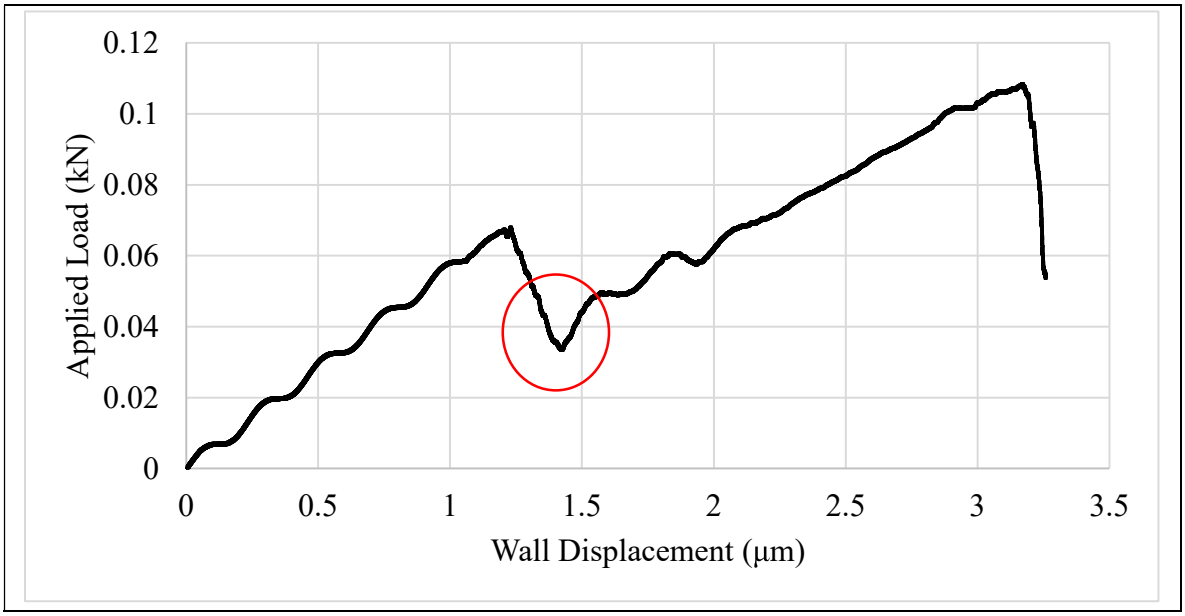

Figure 27. Force – Displacement Graph for CMHB – Granite Sample

The maximum force recorded for Superpave and CMHB mixtures with low angularity is shown in Figure 28. The variability of the maximum force for these type of mixtures was from 0.09 and up to 0.6 kN. Most of the simulations fell between an average angularity of 1400 and 1500. The CMHB sample results are well spread in terms of the average angularity index and the maximum force. The Superpave simulations are mainly concentrated within an average angularity index from 1400 to 1500, and most of their simulations yield a performance above 0.2 kN for the maximum force. To avoid repetition, the following examples include low angularity index in their mixtures.